Application of NEGF and NEGF+DFT to Spin-Orbit Torque and Electron or Magnon Mediated Spin-Transfer Torque

Branislav K. Nikolić

Department of Physics & Astronomy, University of Delaware, Newark, DE 19716, U.S.A.

https://wiki.physics.udel.edu/phys824

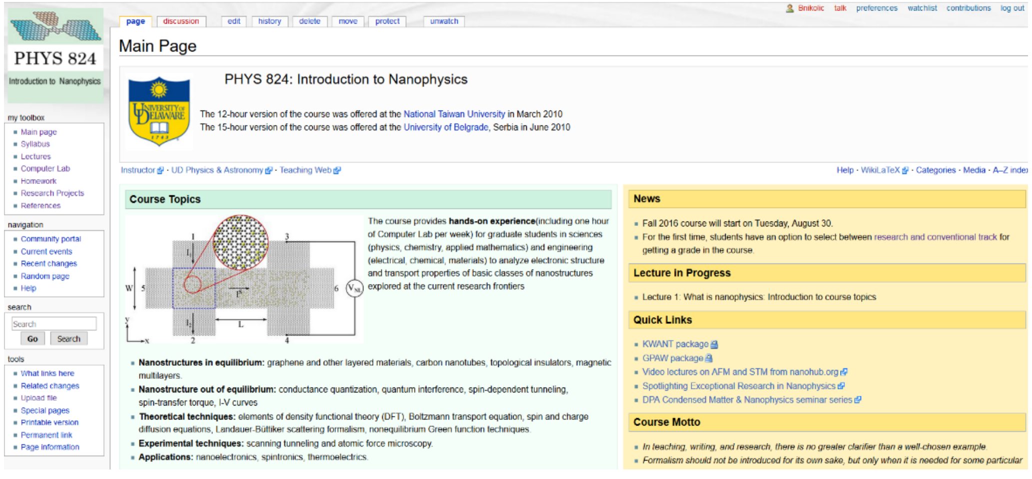

Spin-Transfer Torque (STT): Fundamentals and Applications

Fundamentals

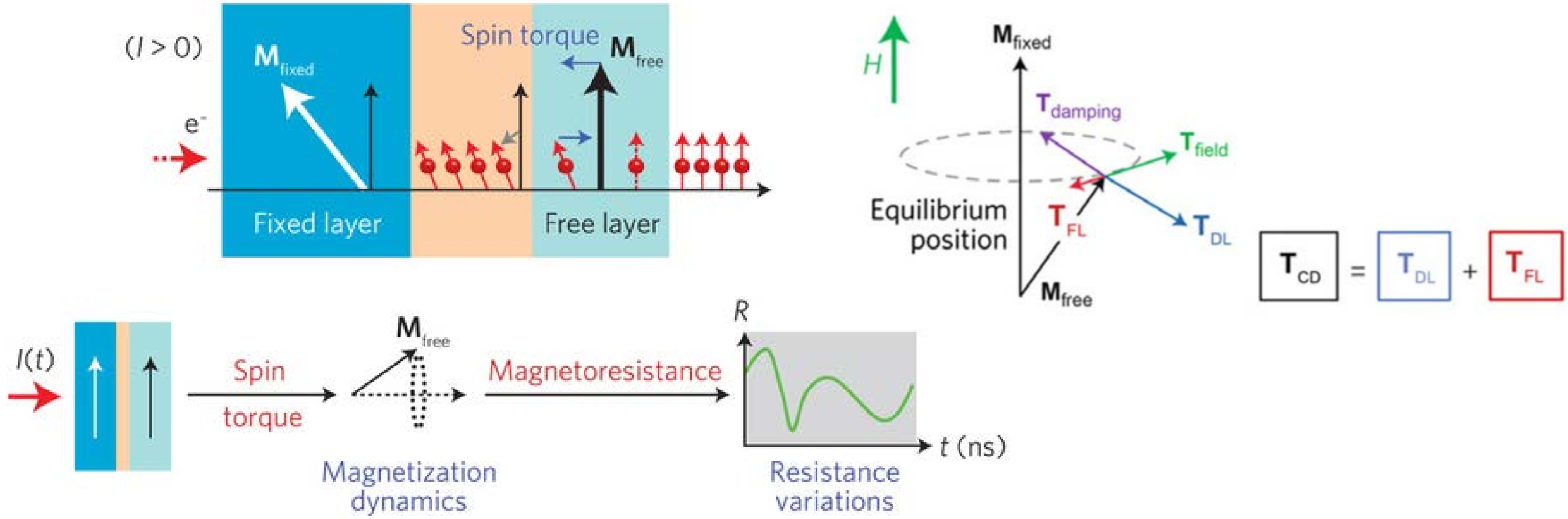

Applications

nature materials | PROGRESS ARTICLE

PUBLISHED ONLINE: 17 DECEMBER 2013 | DOI: 10.1038/NMAT3823

Spin-torque building blocks

N. Locatelli, V. Cros and J. Grollier*

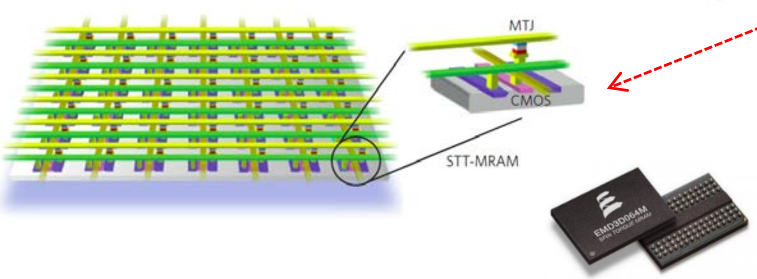

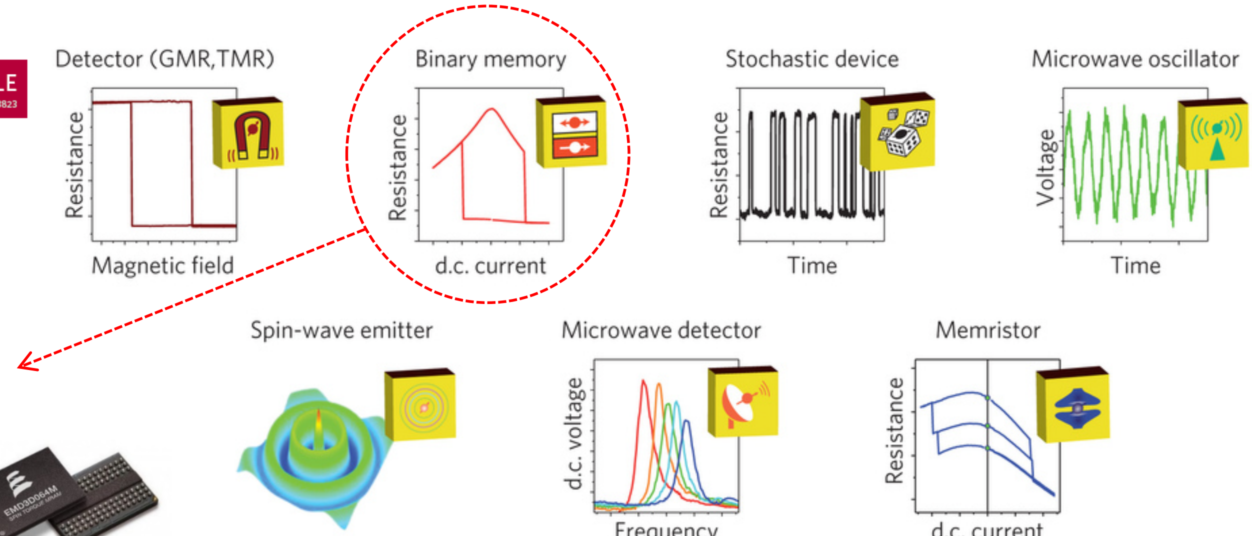

STT-Driven Magnetization is Treated as Classical Vector Obeying Landau-Lifshitz-Gilbert (LLG) Equation

$$\frac{d\mathbf{M}_{\text{free}}}{dt} = -\gamma \mathbf{M}_{\text{free}} \times \mathbf{H}_{eff} + \alpha \mathbf{M}_{\text{free}} \times \frac{d\mathbf{M}_{\text{free}}}{dt} + \mathbf{T}_{\text{DL}} + \mathbf{T}_{\text{FL}}$$

LLG is strictly valid in the classical limit:

$$S \to \infty, \hbar \to 0, S\hbar \to 1$$

$$|\text{FM}\rangle = |\sigma_1\rangle \otimes |\sigma_2\rangle \otimes \cdots \otimes |\sigma_N\rangle$$

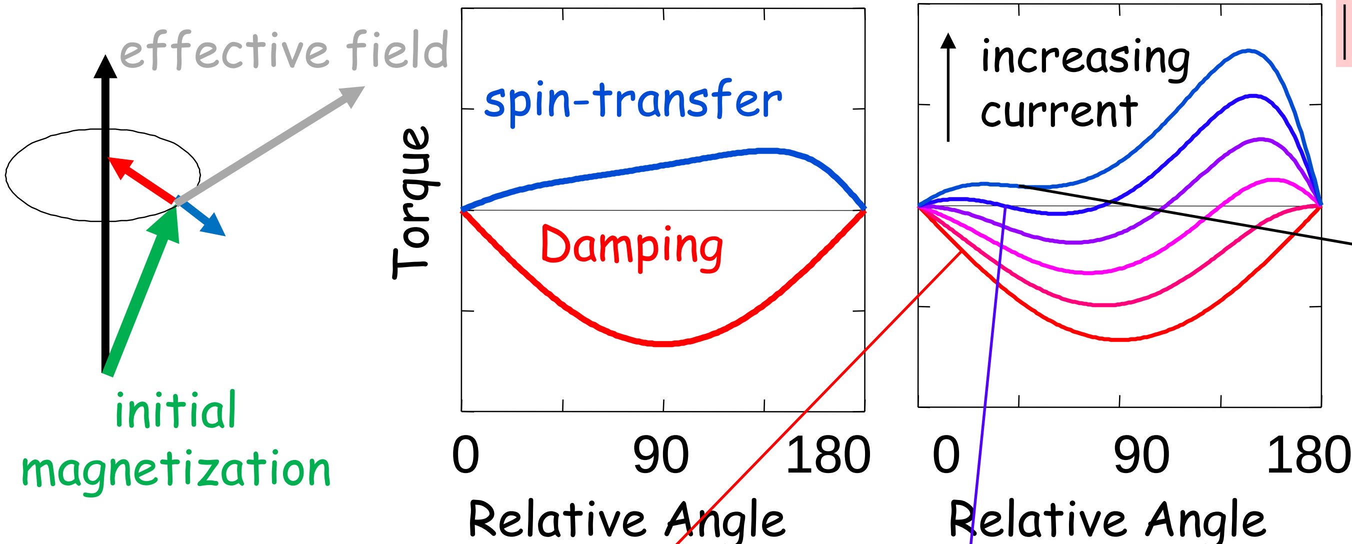

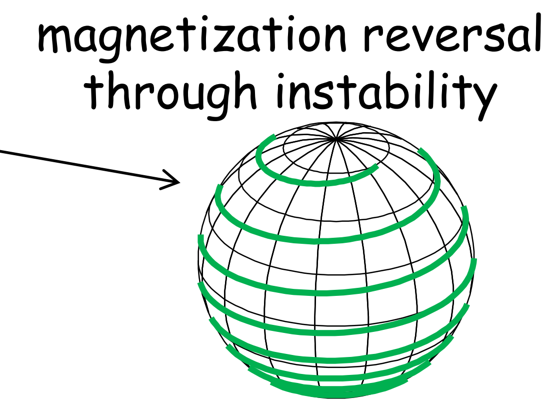

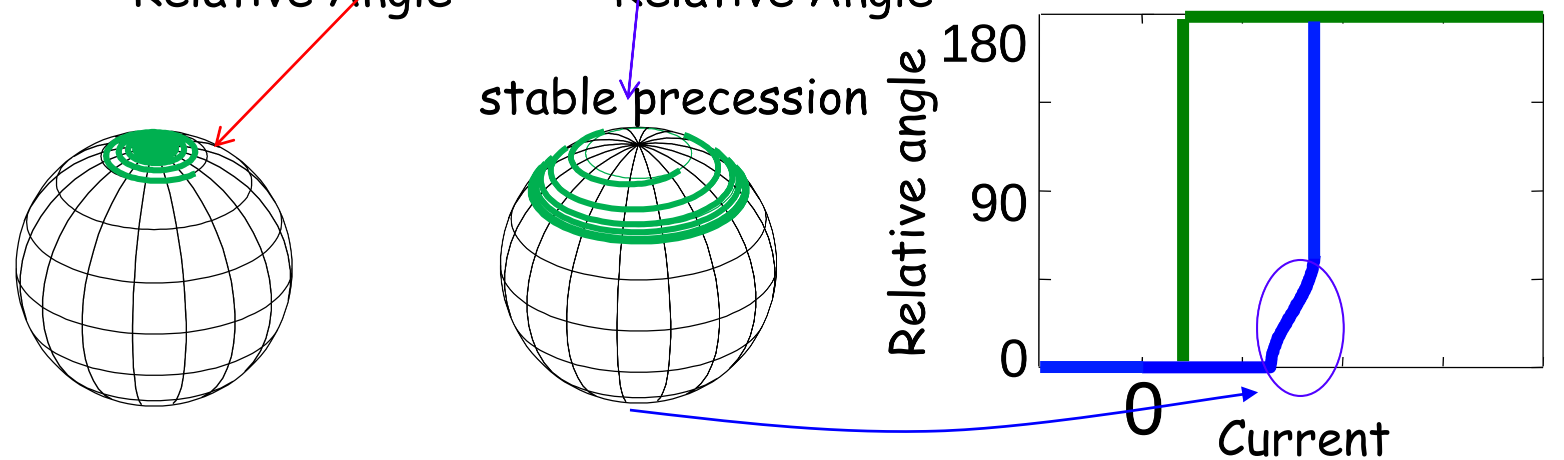

Experimental Manifestations of STT

Journal of Magnetism and Magnetic Materials 320 (2008) 1190–1216

Current Perspectives

Spin transfer torques

D.C. Ralph[a,*], M.D. Stiles[b]

Magnetization Switching

20 nm $Ni_{81}Fe_{19}$ / 12 nm Cu / 4.5 nm $Ni_{81}Fe_{19}$.

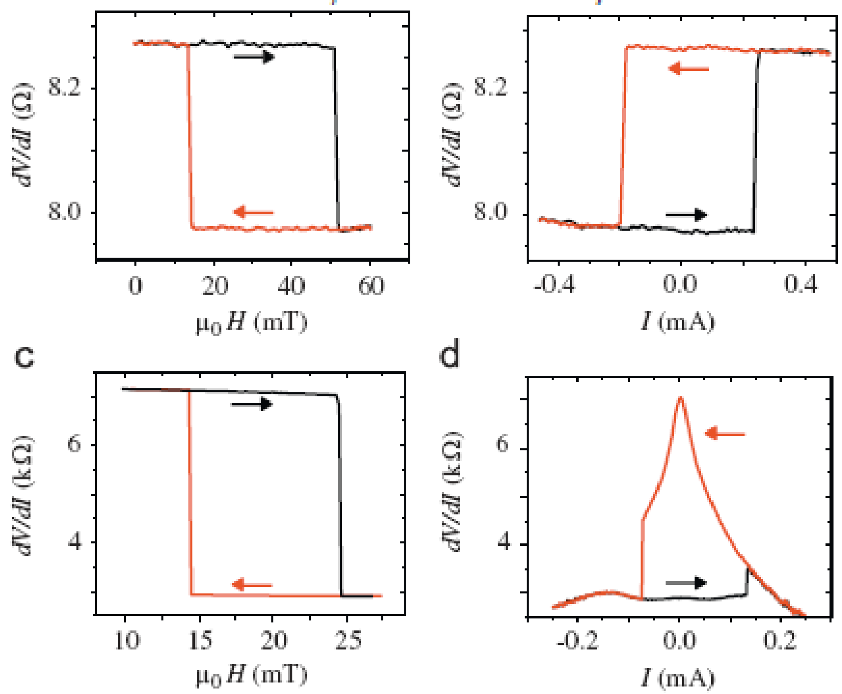

Magnetization Precession

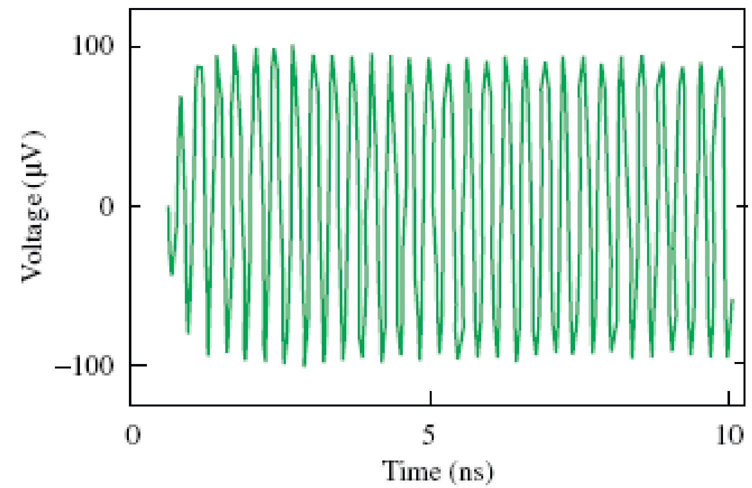

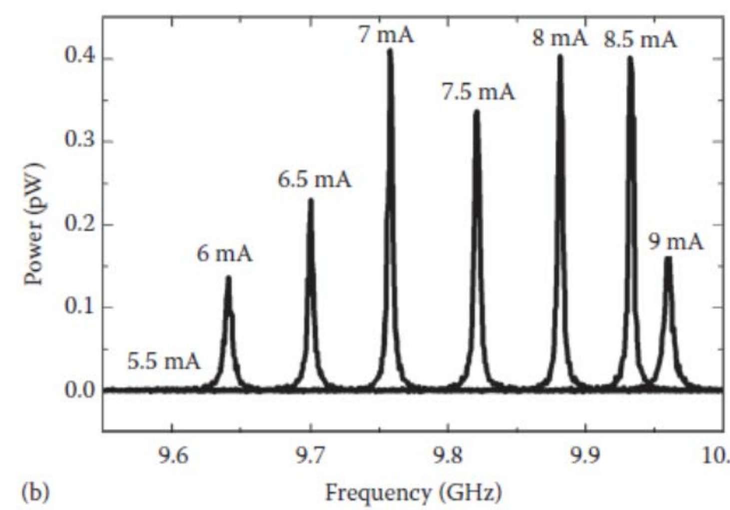

Nat. Mater. 6, 447 (2007)

Elementary Quantum Mechanics of STT: Toy Model #1

$$\psi = \frac{e^{ikx}}{\sqrt{\Omega}}\left(a\left|\uparrow\right\rangle + b\left|\downarrow\right\rangle\right)$$

$$\mathbf{Q} = \frac{\hbar^2}{2m}\mathrm{Im}(\psi^* \boldsymbol{\sigma} \otimes \boldsymbol{\nabla}\psi)$$

$$Q_{xx} = \frac{\hbar^2 k}{2m\Omega}2\mathrm{Re}(ab^*)$$

$$Q_{xy} = \frac{\hbar^2 k}{2m\Omega}2\mathrm{Im}(ab^*)$$

$$Q_{xz} = \frac{\hbar^2 k}{2m\Omega}(|a|^2 - |b|^2)$$

Toy model #1

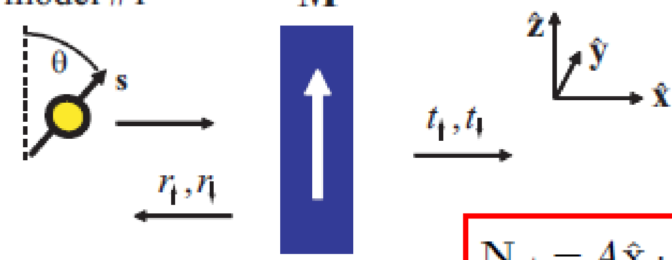

$$\mathbf{N}_{\mathrm{st}} = -\int_{\text{pillbox surfaces}} d^2R\,\hat{\mathbf{n}}\cdot\mathbf{Q} = -\int_{\text{pillbox volume}} d^3r\,\nabla\cdot\mathbf{Q},$$

$$\begin{aligned}\mathbf{N}_{\mathrm{st}} &= A\hat{\mathbf{x}}\cdot(\mathbf{Q}_{\mathrm{in}} + \mathbf{Q}_{\mathrm{refl}} - \mathbf{Q}_{\mathrm{trans}}) \\ &= \frac{A}{\Omega}\frac{\hbar^2 k}{2m}\sin(\theta)\left[1 - \mathrm{Re}(t_\uparrow t_\downarrow^* + r_\uparrow r_\downarrow^*)\right]\hat{\mathbf{x}} \\ &\quad - \frac{A}{\Omega}\frac{\hbar^2 k}{2m}\sin(\theta)\mathrm{Im}(t_\uparrow t_\downarrow^* + r_\uparrow r_\downarrow^*)\hat{\mathbf{y}}.\end{aligned}$$

$$\psi_{\mathrm{in}} = \frac{e^{ikx}}{\sqrt{\Omega}}\left(\cos(\theta/2)\left|\uparrow\right\rangle + \sin(\theta/2)\left|\downarrow\right\rangle\right)$$

$$\psi_{\mathrm{trans}} = \frac{e^{ikx}}{\sqrt{\Omega}}\left(t_\uparrow\cos(\theta/2)\left|\uparrow\right\rangle + t_\downarrow\sin(\theta/2)\left|\downarrow\right\rangle\right)$$

$$\psi_{\mathrm{refl}} = \frac{e^{-ikx}}{\sqrt{\Omega}}\left(r_\uparrow\cos(\theta/2)\left|\uparrow\right\rangle + r_\downarrow\sin(\theta/2)\left|\downarrow\right\rangle\right)$$

$$\mathbf{Q}_{\mathrm{in}} = \frac{\hbar^2 k}{2m\Omega}\left[\sin(\theta)\hat{\mathbf{x}} + \cos(\theta)\hat{\mathbf{z}}\right]$$

$$\begin{aligned}\mathbf{Q}_{\mathrm{trans}} &= \frac{\hbar^2 k}{2m\Omega}\sin(\theta)\mathrm{Re}(t_\uparrow t_\downarrow^*)\hat{\mathbf{x}} \\ &+ \frac{\hbar^2 k}{2m\Omega}\sin(\theta)\mathrm{Im}(t_\uparrow t_\downarrow^*)\hat{\mathbf{y}} \\ &+ \frac{\hbar^2 k}{2m\Omega}\left[|t_\uparrow|^2\cos^2(\theta/2) - |t_\downarrow|^2\sin^2(\theta/2)\right]\hat{\mathbf{z}}\end{aligned}$$

$$\begin{aligned}\mathbf{Q}_{\mathrm{refl}} &= -\frac{\hbar^2 k}{2m\Omega}\sin(\theta)\mathrm{Re}(r_\uparrow r_\downarrow^*)\hat{\mathbf{x}} \\ &- \frac{\hbar^2 k}{2m\Omega}\sin(\theta)\mathrm{Im}(r_\uparrow r_\downarrow^*)\hat{\mathbf{y}} \\ &- \frac{\hbar^2 k}{2m\Omega}\left[|r_\uparrow|^2\cos^2(\theta/2) - |r_\downarrow|^2\sin^2(\theta/2)\right]\hat{\mathbf{z}}\end{aligned}$$

JMMM **320**, 1190 (2008)

Elementary Quantum Mechanics of STT: Toy Model #2

$$\psi_{\rm trans} = \frac{e^{ik_\uparrow x}}{\sqrt{\Omega}}\cos(\theta/2)\,|\uparrow\rangle + \frac{e^{ik_\downarrow x}}{\sqrt{\Omega}}\frac{2k}{k+k_\downarrow}\sin(\theta/2)\,|\downarrow\rangle$$

$$\psi_{\rm refl} = \frac{e^{-ikx}}{\sqrt{\Omega}}\frac{k-k_\downarrow}{k+k_\downarrow}\sin(\theta/2)\,|\downarrow\rangle\,,$$

$$k_\uparrow = k \text{ and } k_\downarrow = [2m(E-\Delta)]^{1/2}/\hbar < k$$

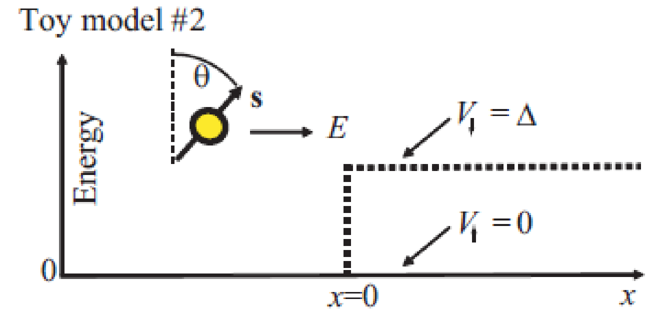

$$\mathbf{Q} = \frac{\hbar^2}{2m}\mathrm{Im}(\psi^*\boldsymbol{\sigma}\otimes\boldsymbol{\nabla}\psi)$$

$$\mathbf{Q}_{\rm in} = \frac{\hbar^2}{2m\Omega}\left(k\sin(\theta)\hat{\mathbf{x}} + k\cos(\theta)\hat{\mathbf{z}}\right)$$

$$\mathbf{Q}_{\rm trans} = \frac{\hbar^2}{2m\Omega}\sin(\theta)k\cos[(k_\uparrow - k_\downarrow)x]\hat{\mathbf{x}} - \frac{\hbar^2}{2m\Omega}\sin(\theta)k\sin[(k_\uparrow - k_\downarrow)x]\hat{\mathbf{y}} + \frac{\hbar^2}{2m\Omega}\left[k\cos^2(\theta/2) - k_\downarrow\left(\frac{2k}{k+k_\downarrow}\right)^2\sin^2(\theta/2)\right]\hat{\mathbf{z}}$$

$$\mathbf{Q}_{\rm refl} = \frac{\hbar^2}{2m\Omega}k\left(\frac{k-k_\downarrow}{k+k_\downarrow}\right)^2\sin^2(\theta/2)\hat{\mathbf{z}}.$$

$$\mathbf{N}_{\rm st} = A\hat{\mathbf{x}}\cdot(\mathbf{Q}_{\rm in} + \mathbf{Q}_{\rm refl} - \mathbf{Q}_{\rm trans}) \approx A\hat{\mathbf{x}}\cdot\mathbf{Q}_{\rm in\perp}$$

$$\mathbf{N}_{\rm st} \approx \frac{A}{\Omega}\frac{\hbar^2 k}{2m}\sin(\theta)\hat{\mathbf{x}}$$

when summing or averaging over all contributions from around the Fermi surface, dephasing leads to Q_{refl}≈0, Q_{trans}≈0 (to a good approximation valid for typical metallic interfaces), so that STT acting on the magnet per unit area being equal to the full component of incident spin current that is transverse to magnetization of free ferromagnetic layer

JMMM **320**, 1190 (2008)

Spin-Transfer and Spin-Orbit Torques from Nonequilibrium Green Functions (NEGF)

❑Fundamental quantities of NEGF formalism:

density of available quantum states:

$$G^r_{\sigma\sigma'}(t,t') = -\frac{i}{\hbar}\Theta(t-t')\langle\{\hat{c}_{\mathbf{r}\sigma}(t), \hat{c}^\dagger_{\mathbf{r}'\sigma'}(t')\}\rangle$$

how are those states occupied:

$$G^<_{\sigma\sigma'}(t,t') = \frac{i}{\hbar}\langle\hat{c}^\dagger_{\mathbf{r}'\sigma'}(t')\hat{c}_{\mathbf{r}\sigma}(t)\rangle$$

Learn more about NEGF from:

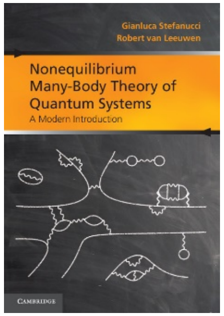

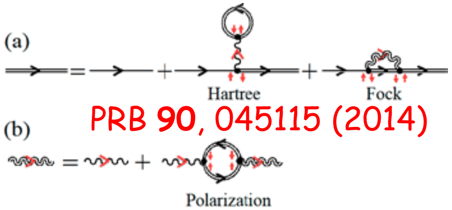

PRB **90**, 045115 (2014)

❑NEGF for steady-state transport:

$$G^r(t,t') \rightarrow G^r(t-t') \xrightarrow{\mathrm{FT}} G^r(E)$$

$$G^<(t,t') \rightarrow G^<(t-t') \xrightarrow{\mathrm{FT}} G^<(E)$$

$$\boldsymbol{\rho}_{\mathrm{eq}} = -\frac{1}{\pi}\int_{-\infty}^{+\infty} dE\, \mathrm{Im}\,\mathbf{G}^r(E) f(E-E_F)$$

$$\boldsymbol{\rho}_{\mathrm{neq}} = \frac{1}{2\pi i}\int_{-\infty}^{+\infty} dE\, \mathbf{G}^<(E)$$

❑NEGF-based expression for spin-transfer torque:

First-Principles Quantum Transport Modeling of Spin-Transfer and Spin-Orbit Torques in Magnetic Multilayers

Branislav K. Nikolić, Kapildeb Dolui, Marko D. Petrović, Petr Plecháč, Troels Markussen, and Kurt Stokbro

PHYSICAL REVIEW MATERIALS 3, 011401(R) (2019)

Rapid Communications

First-principles calculation of spin-orbit torque in a Co/Pt bilayer

K. D. Belashchenko,[1] Alexey A. Kovalev,[1] and M. van Schilfgaarde[2]

LCAO-ncDFT from:

SYNOPSYS | QuantumATK

$$\hat{H} = -\frac{\hbar^2\nabla^2}{2m} + V_{\mathrm{H}}(\mathbf{r}) + V_{\mathrm{XC}}(\mathbf{r}) + V_{\mathrm{ext}}(\mathbf{r}) - \boldsymbol{\sigma}\cdot\mathbf{B}_{\mathrm{XC}}(\mathbf{r}) \Rightarrow \hat{\mathbf{T}} = \frac{d\hat{\mathbf{S}}}{dt} = \frac{1}{2i}[\hat{\boldsymbol{\sigma}}, \hat{H}]$$

$$\mathbf{T} = \mathrm{Tr}\,[\hat{\rho}_{\mathrm{neq}}\hat{\mathbf{T}}] \Leftrightarrow \mathbf{T} = \int_F d^3r\, \mathbf{m}_{\mathrm{neq}}(\mathbf{r}) \times \mathbf{B}_{\mathrm{XC}}(\mathbf{r})$$

most general torque formula valid in the presence of SOC and other spin-nonconserving processes

EXAMPLE: NEGF+DFT Theory of STT in Co/Cu/Co Spin Valve

First-Principles Quantum Transport Modeling of Spin-Transfer and Spin-Orbit Torques in Magnetic Multilayers

Branislav K. Nikolić, Kapildeb Dolui, Marko D. Petrović, Petr Plecháč, Troels Markussen, and Kurt Stokbro

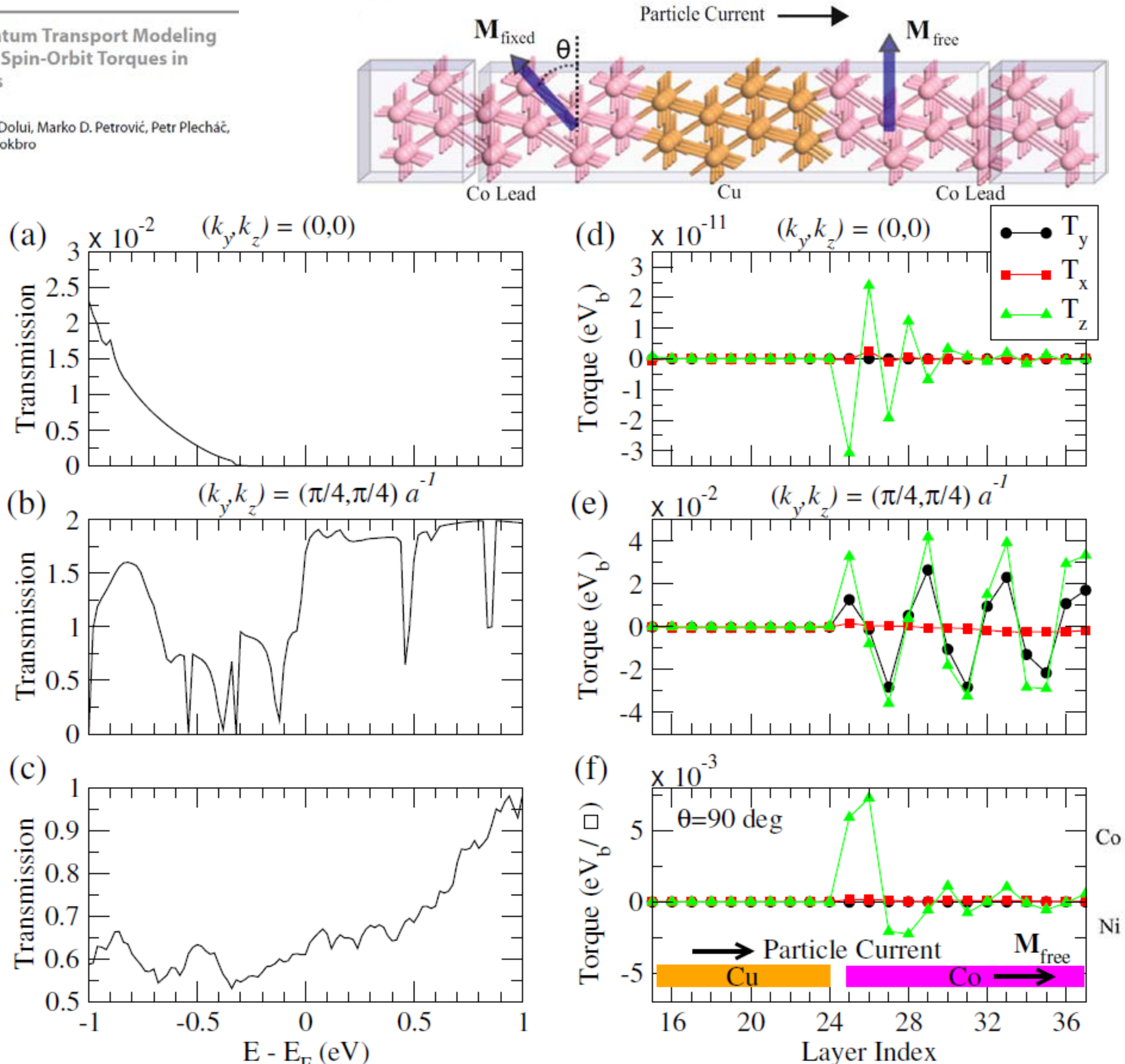

PRB **77**, 184430 (2008)

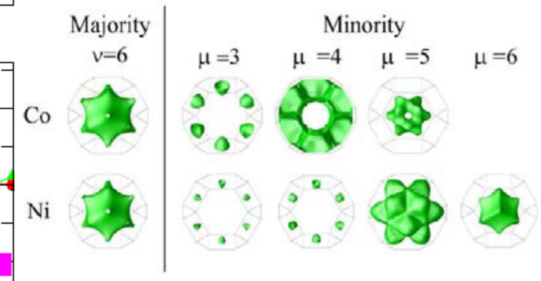

Spin-Orbit Torque (SOT): Fundamentals and Applications

Fundamentals

Nat. Mater. **12**, 240 (2013)

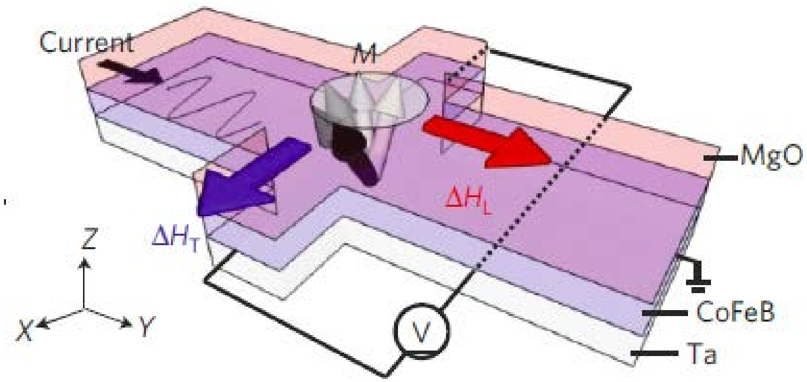

Nat. Nanotech. **14**, 945 (2019)

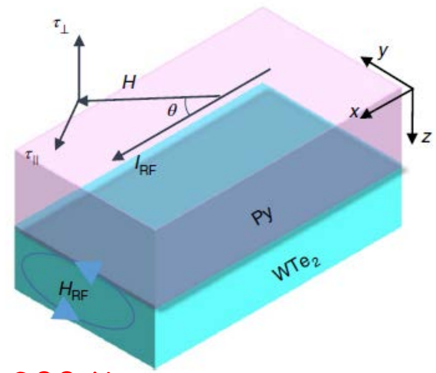

T=300 K
Magnetization switching with ultralow current density ~3×10^5 A/cm^2

Nano Lett. **19**, 4400 (2019)
Sci. Adv. **5**, eaaw8904 (2019)

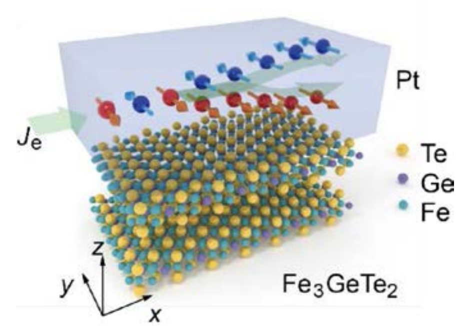

T~225 K
Switching with current density ~3×10^7 A/cm^2 **but gate tunable**

Applications

JPDAP **51**, 273002 (2018)

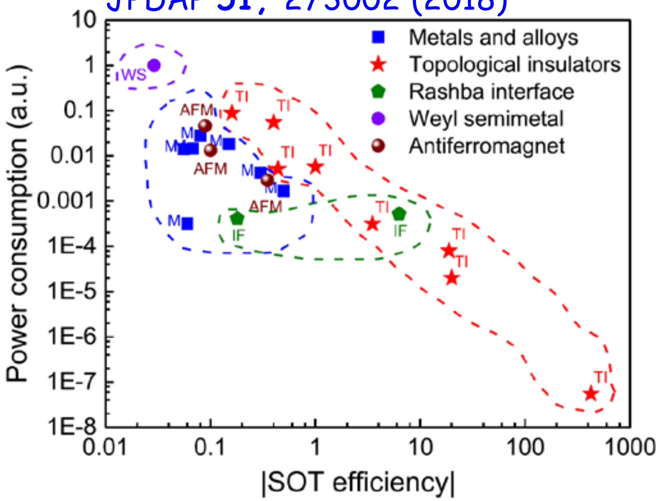

high efficiency of SOT-driven magnetization switching demonstrated: 60 fJ (vs. 150 fJ to 4 pJ with STT) energy consumed per bit writing

solid-state nonvolatile analogue memory with infinite read-write endurance

Applied Physics Express **10**, 013007 (2017)
https://doi.org/**10.7567/APEX.10.013007**

Analogue spin–orbit torque device for artificial-neural-network-based associative memory operation

William A. Borders[1], Hisanao Akima[1*], Shunsuke Fukami[1,2,3,4*], Satoshi Moriya[1], Shouta Kurihara[1], Yoshihiko Horio[1], Shigeo Sato[1], and Hideo Ohno[1,2,3,4,5]

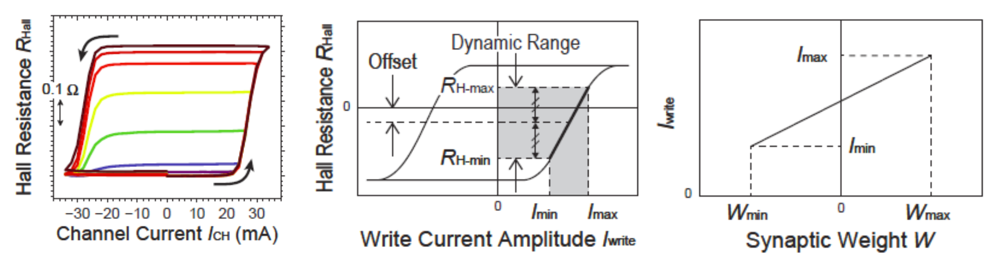

Experimental Probing of Spatially and Time-Resolved SOT-Driven Magnetization Switching

ARTICLES
nature nanotechnology
PUBLISHED ONLINE: 21 AUGUST 2017 | DOI: 10.1038/NNANO.2017.151

Spatially and time-resolved magnetization dynamics driven by spin–orbit torques

Manuel Baumgartner[1]*, Kevin Garello[1,2]*, Johannes Mendil[1], Can Onur Avci[1], Eva Grimaldi[1], Christoph Murer[1], Junxiao Feng[1], Mihai Gabureac[1], Christian Stamm[1], Yves Acremann[3], Simone Finizio[4], Sebastian Wintz[4], Jörg Raabe[4] and Pietro Gambardella[1]*

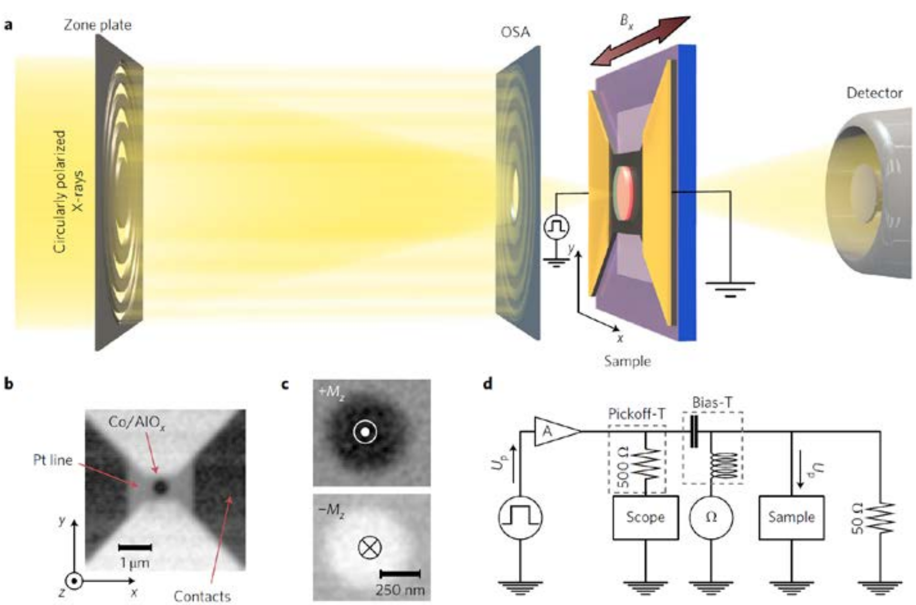

Experiment

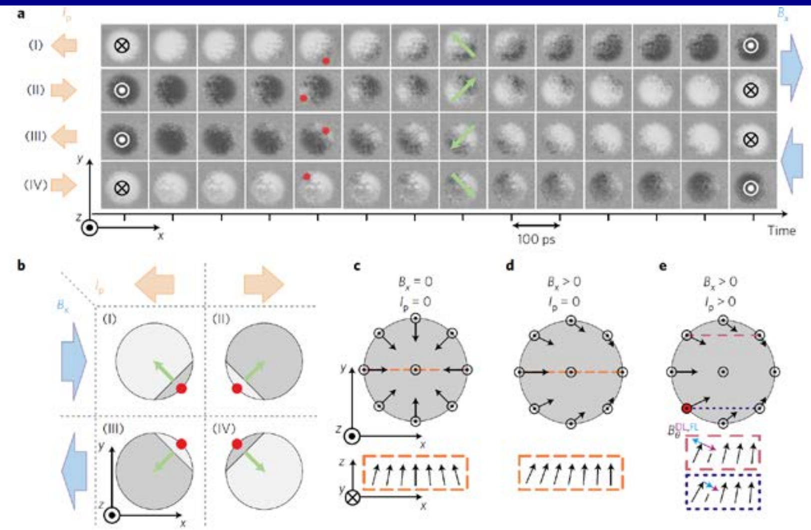

Figure 3 | Evolution of the magnetization during the switching process. a, Images taken at intervals of 100 ps during the injection of 2-ns-long current pulses. I_p indicates the direction of the current pulse. Rows (I,II) and (III,IV) correspond to the time traces shown in Fig. 2a,b, respectively. The red dots indicate the domain wall nucleation point and the green arrows its propagation direction. The images are low-pass filtered for better contrast (see Supplementary Fig. 10 and the Supplementary Information for the raw data and movies). **b**, Schematic of the observed domain wall nucleation and propagation geometry. **c–e**, Illustration of the nucleation process corresponding to case (II). **c**, Canting of the magnetization at the dot edges induced by the DMI. **d**, Breaking of the canting symmetry induced by B_x. **e**, Action of B_θ^{DL} and B_θ^{FL}.

Micromagnetic simulations

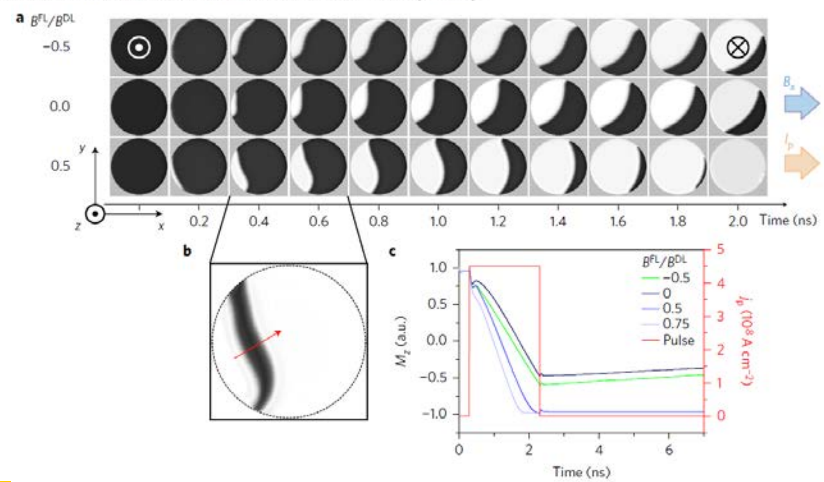

Crash Course on Spin-Orbit Coupling (SOC) in Vacuum

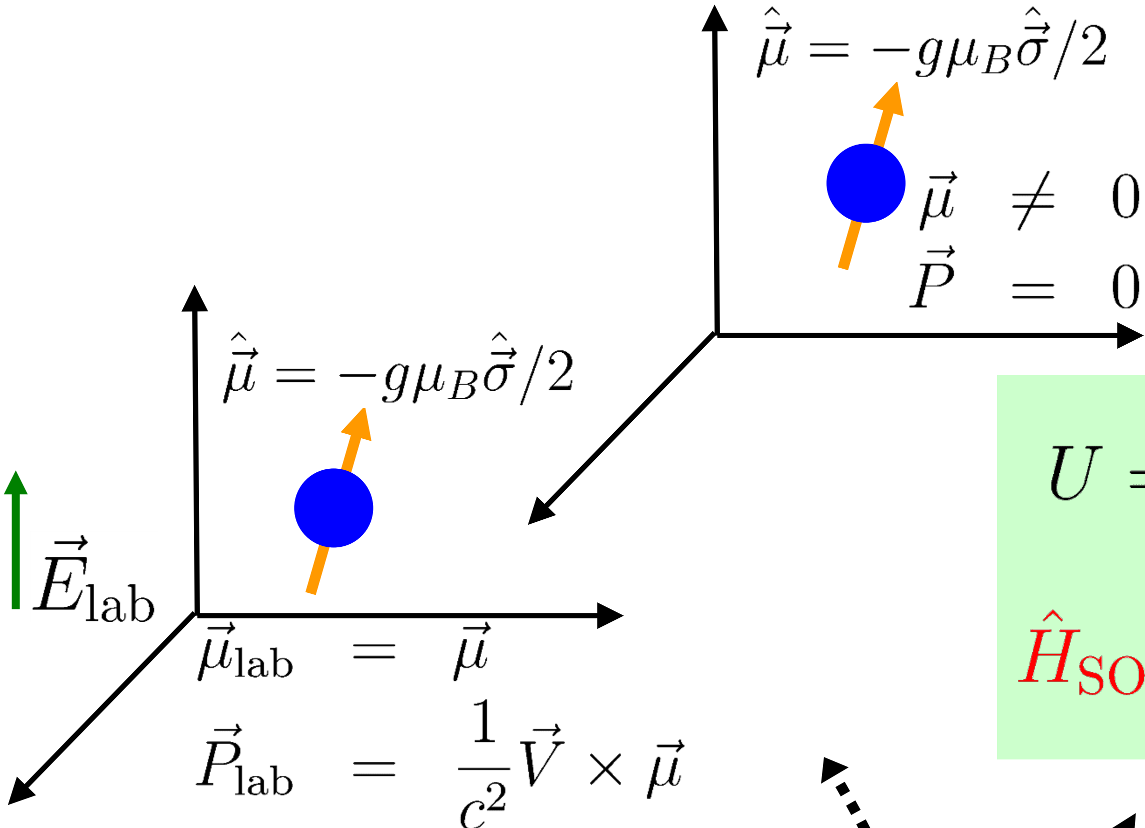

$$U = -\frac{1}{2}\vec{P}_{\text{lab}} \cdot \vec{E}$$

$$\hat{H}_{\text{SO}} = \frac{e\hbar^2}{4m_0^2c^2}(\hat{\vec{\sigma}} \times \hat{\vec{p}}) \cdot \vec{E}$$

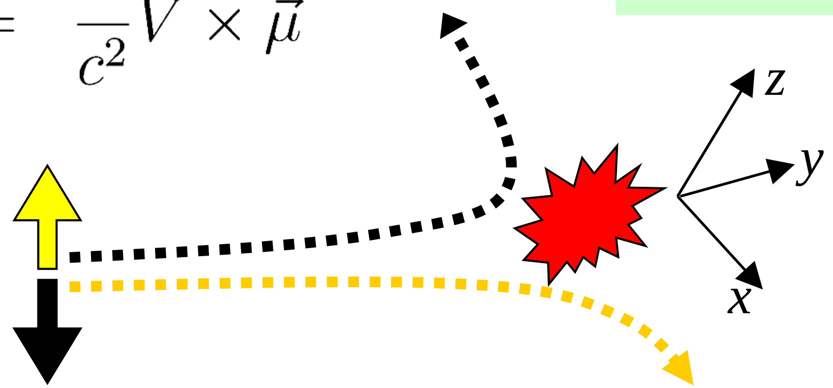

SO deflection force:

$$F_{\text{SO}} = \pm P_{\text{lab}} \nabla E_x$$

Crash Course on Rashba SOC in Solids

$$\hat{H}^{\mathrm{R}}_{\mathrm{SO}} = \frac{\alpha}{\hbar}(\hat{\boldsymbol{\sigma}} \times \hat{\mathbf{p}}) \cdot \mathbf{e}_z \equiv -\frac{g\mu_B}{2}\hat{\boldsymbol{\sigma}} \cdot \mathbf{B}_{\mathrm{R}}(\hat{\mathbf{p}})$$

$E(k_x)$

1D:

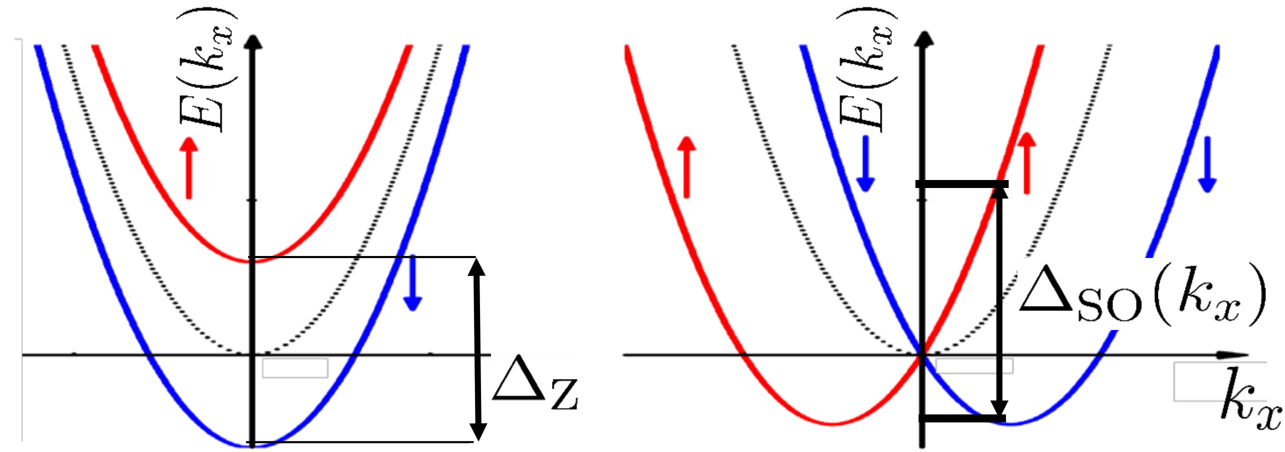

2D:

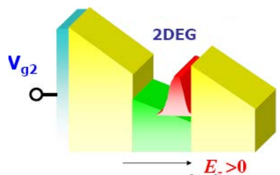

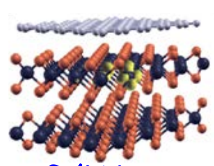

G/WS$_2$

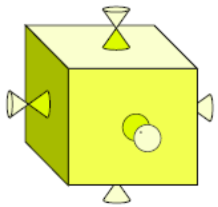

$$\varepsilon(\mathbf{k},\uparrow) = \varepsilon(-\mathbf{k},\downarrow)$$

$$\varepsilon(\mathbf{k},\uparrow) \neq \varepsilon(-\mathbf{k},\uparrow)$$

$$\varepsilon(\mathbf{k},\uparrow) \neq \varepsilon(\mathbf{k},\downarrow)$$

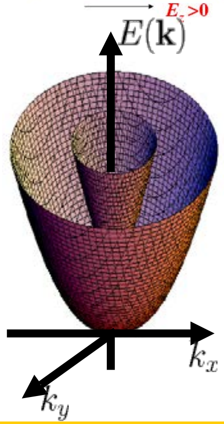

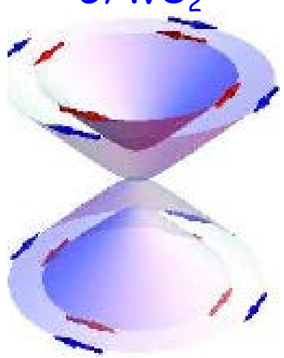

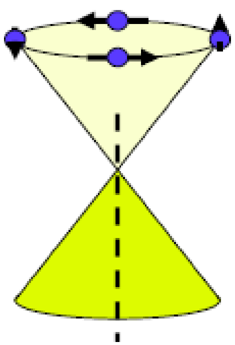

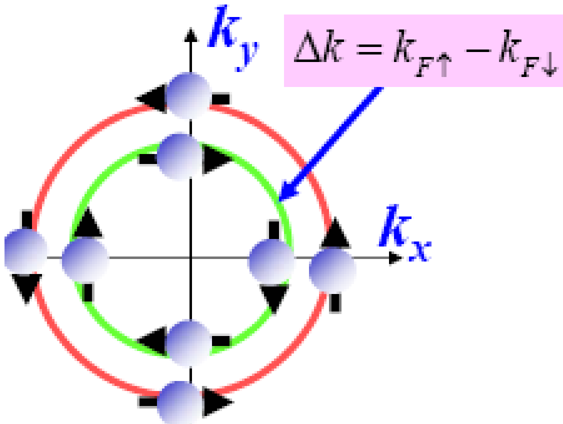

Current-Driven Nonequilibrium Spin Density in the Presence of SOC as the Origin of Field-like SOT

Solid State Communications, Vol. 73, No. 3, pp. 233–235, 1990. 0038–1098/90 $3.00 + .00
Printed in Great Britain. Pergamon Press plc

SPIN POLARIZATION OF CONDUCTION ELECTRONS INDUCED BY ELECTRIC CURRENT IN TWO-DIMENSIONAL ASYMMETRIC ELECTRON SYSTEMS

V.M. Edelstein

USSR Academy of Sciences, Institute of Solid State Physics, Chernogolovka 142432, USSR

nature materials | INSIGHT | PROGRESS ARTICLE
PUBLISHED ONLINE: 23 APRIL 2012 | DOI: 10.1038/NMAT3305

Spintronics and pseudospintronics in graphene and topological insulators

Dmytro Pesin and Allan H. MacDonald

$$S_y = \beta E_x$$

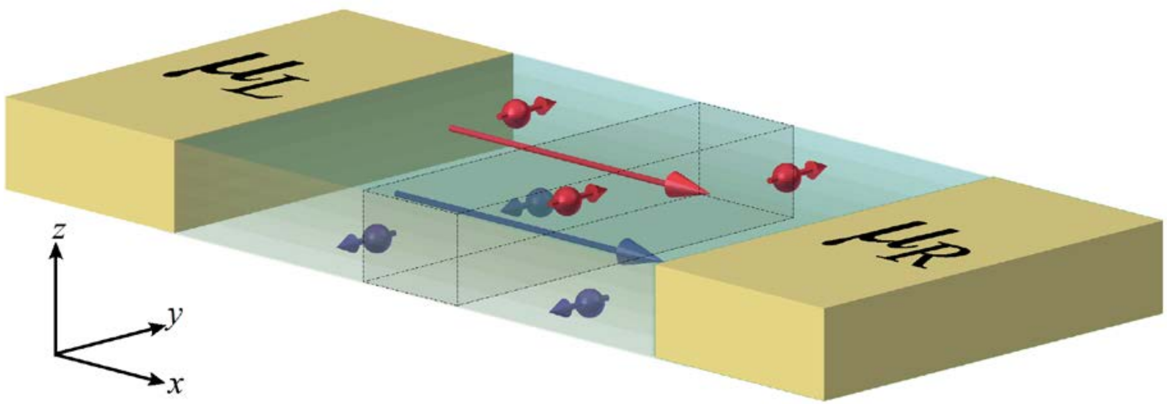

$$\frac{S_y^{\mathrm{Rashba}}}{n} = \frac{e\tau E_x}{p_F}\frac{\alpha}{\hbar v_F} \quad \text{vs.} \quad \frac{S_y^{\mathrm{TI}}}{n} = \frac{e\tau E_x}{p_F}$$

EXAMPLE: Current-Driven Nonequilibrium Spin Density around the Surface of Bi_2Se_3

PRB **92**, 201406(R) (2015)

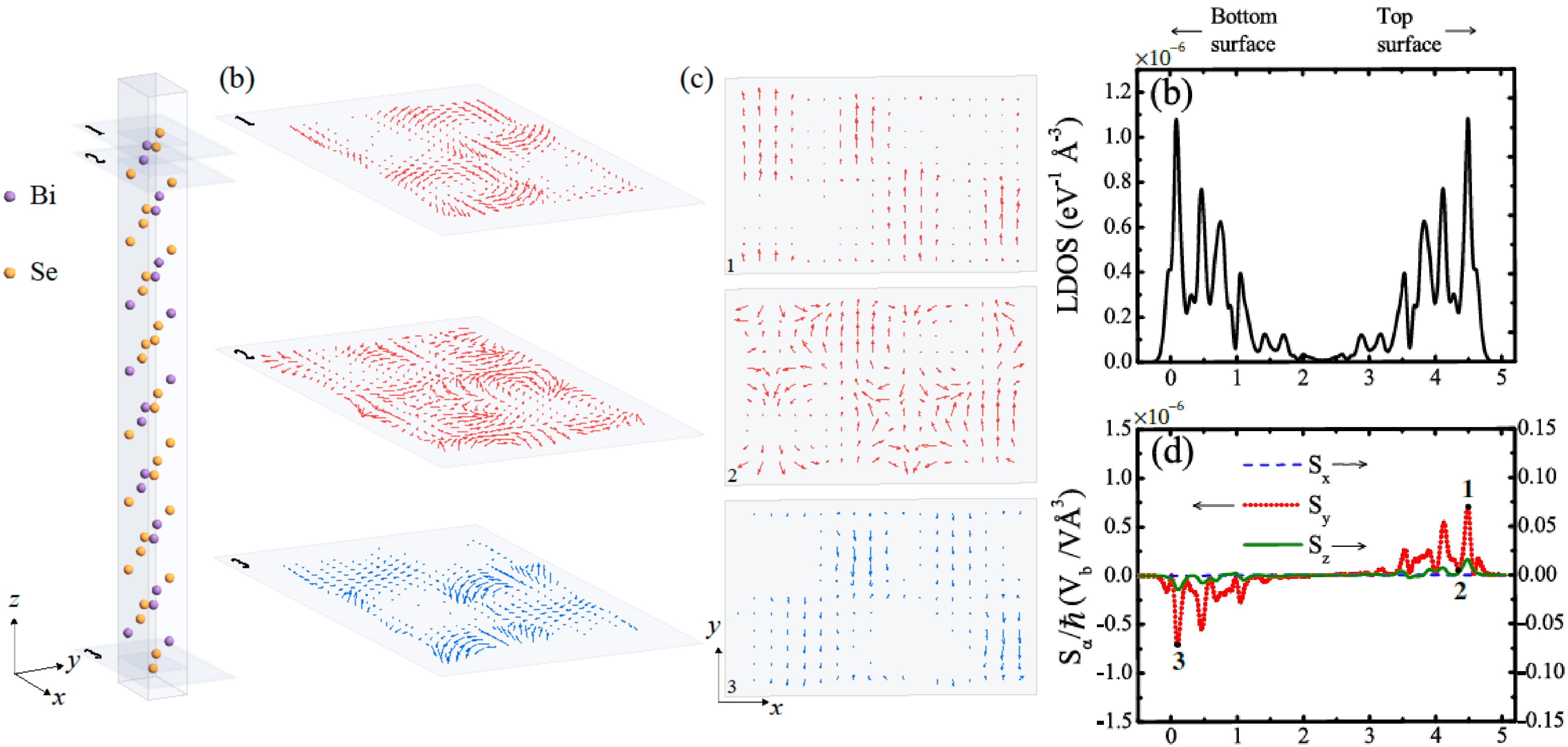

Trouble with Simplistic Hamiltonians for Describing SOT Experiments

LETTER 24 JULY 2014 | VOL 511 | NATURE | 449
doi:10.1038/nature13534

Spin-transfer torque generated by a topological insulator

A. R. Mellnik[1], J. S. Lee[2], A. Richardella[2], J. L. Grab[1], P. J. Mintun[1], M. H. Fischer[1,3], A. Vaezi[1], A. Manchon[4], E.-A. Kim[1], N. Samarth[2] & D. C. Ralph[1,5]

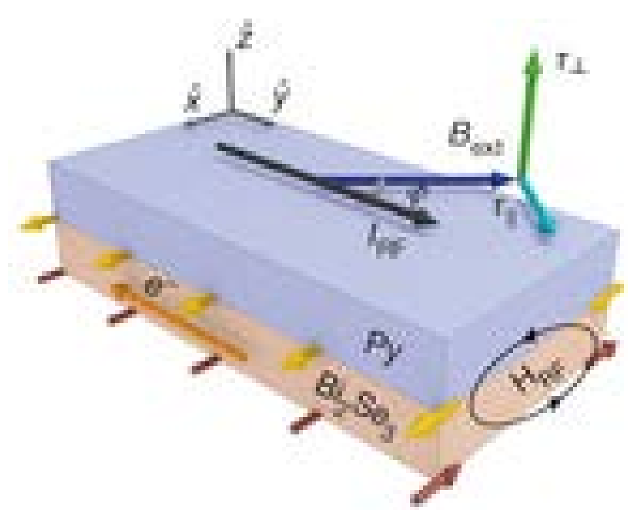

Table 1 | Comparison of room-temperature $\sigma_{s,\parallel}$ and $\theta_{s,\parallel}$ for Bi_2Se_3 with other materials

Parameter	Bi_2Se_3 (this work)	Pt (ref. 4)	β-Ta (ref. 6)	Cu(Bi) (ref. 23)	β-W (ref. 24)
$\theta_\parallel$	2.0–3.5	0.08	0.15	0.24	0.3
$\sigma_{S,\parallel}$	1.1–2.0	3.4	0.8	—	1.8

$\theta_\parallel$ is dimensionless and the units for $\sigma_{S,\parallel}$ are $10^5\hbar/2e\ \Omega^{-1}\ m^{-1}$.

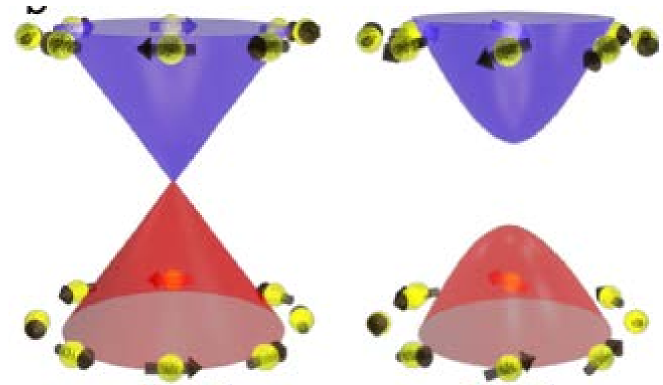

"Our findings have potential importance for technology, in that the spin torque ratio for Bi_2Se_3 at room temperature is larger than that for any previously measured spin current source material. However, as noted above, for practical applications the specific layer structure of our devices (topological insulator/metallic magnet) does not make good use of this high intrinsic efficiency because most of the applied current is shunted through the metallic magnet and does not contribute to spin current generation within the topological insulator. Applications will probably require coupling topological insulators to insulating (or high-resistivity) magnets so that the majority of the current will flow in the topological insulator."

Spin-Orbit-Proximitized Ferromagnet: Co/Topological-Insulator-Bi_2Se_3

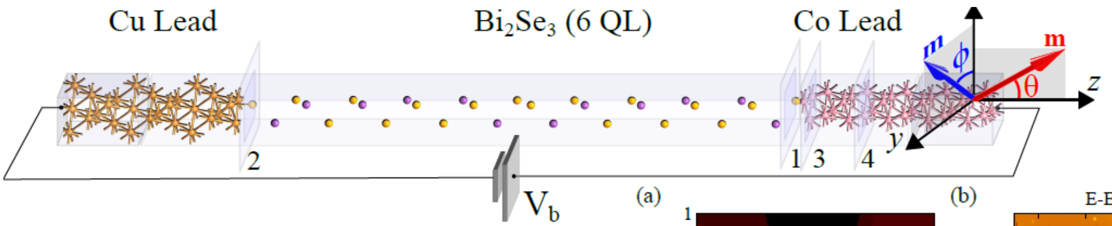

$$A(E; k_x, k_y, z) = -\frac{1}{\pi}\mathrm{Im}\left[G_{\mathbf{k}_\parallel}(E; z, z)\right]$$

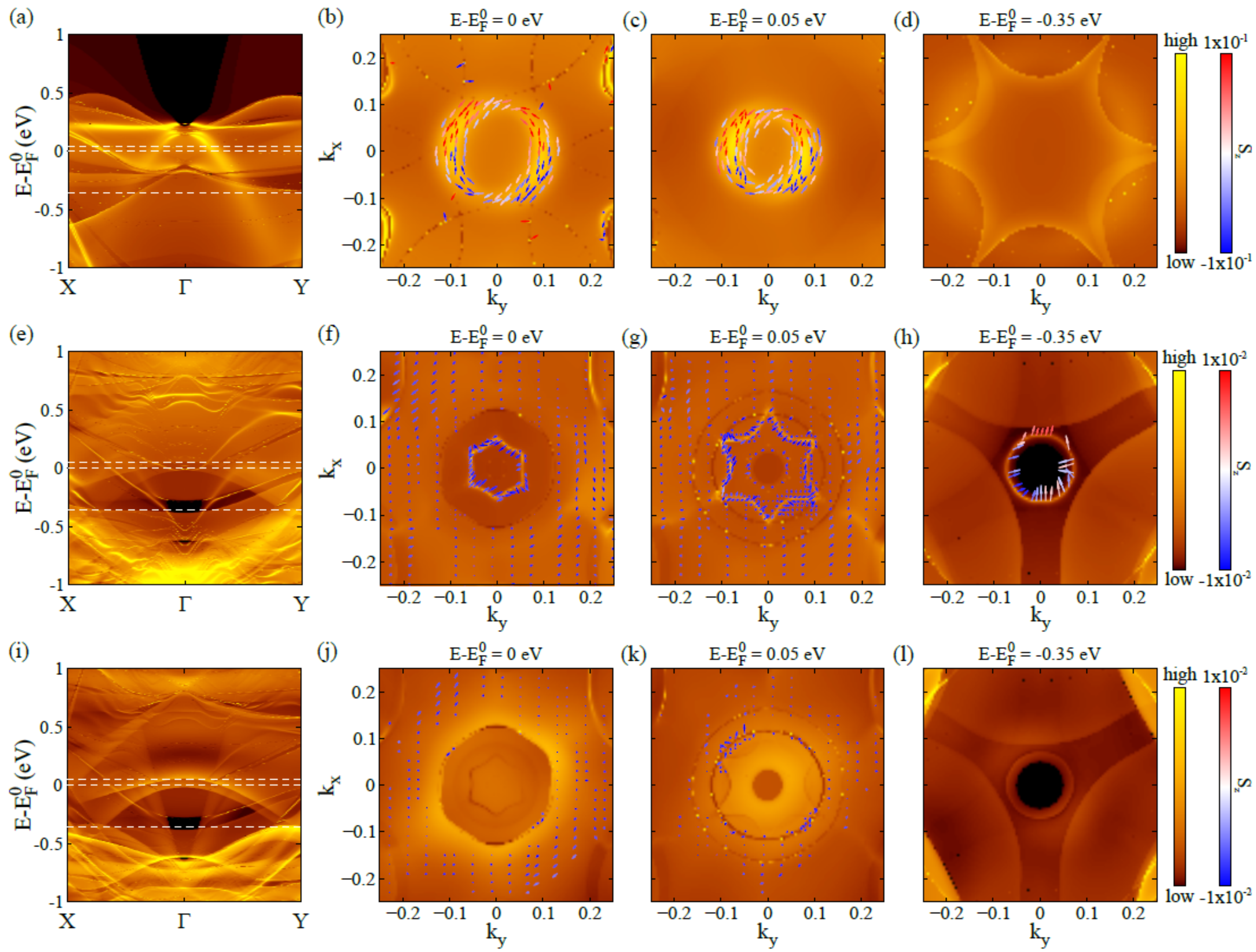


NANO LETTERS
Letter
pubs.acs.org/NanoLett

Proximity Band Structure and Spin Textures on Both Sides of Topological-Insulator/Ferromagnetic-Metal Interface and Their Charge Transport Probes

Juan Manuel Marmolejo-Tejada,[†,∥] Kapildeb Dolui,[†] Predrag Lazić,[‡] Po-Hao Chang,[¶] Søren Smidstrup,[§] Daniele Stradi,[§] Kurt Stokbro,[§] and Branislav K. Nikolić[*,†]

Nano Lett. **17**, 5626 (2017)

Spectral Function on the TI Side of Co/TI Interface

Nano Lett. **17**, 5626 (2017)

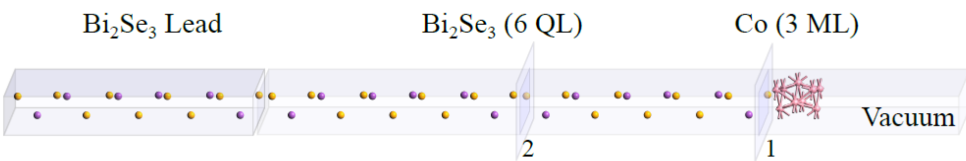

PRB **82**, 195417 (2010)
PRB **96**, 235433 (2017)

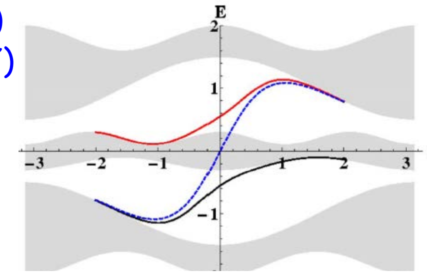

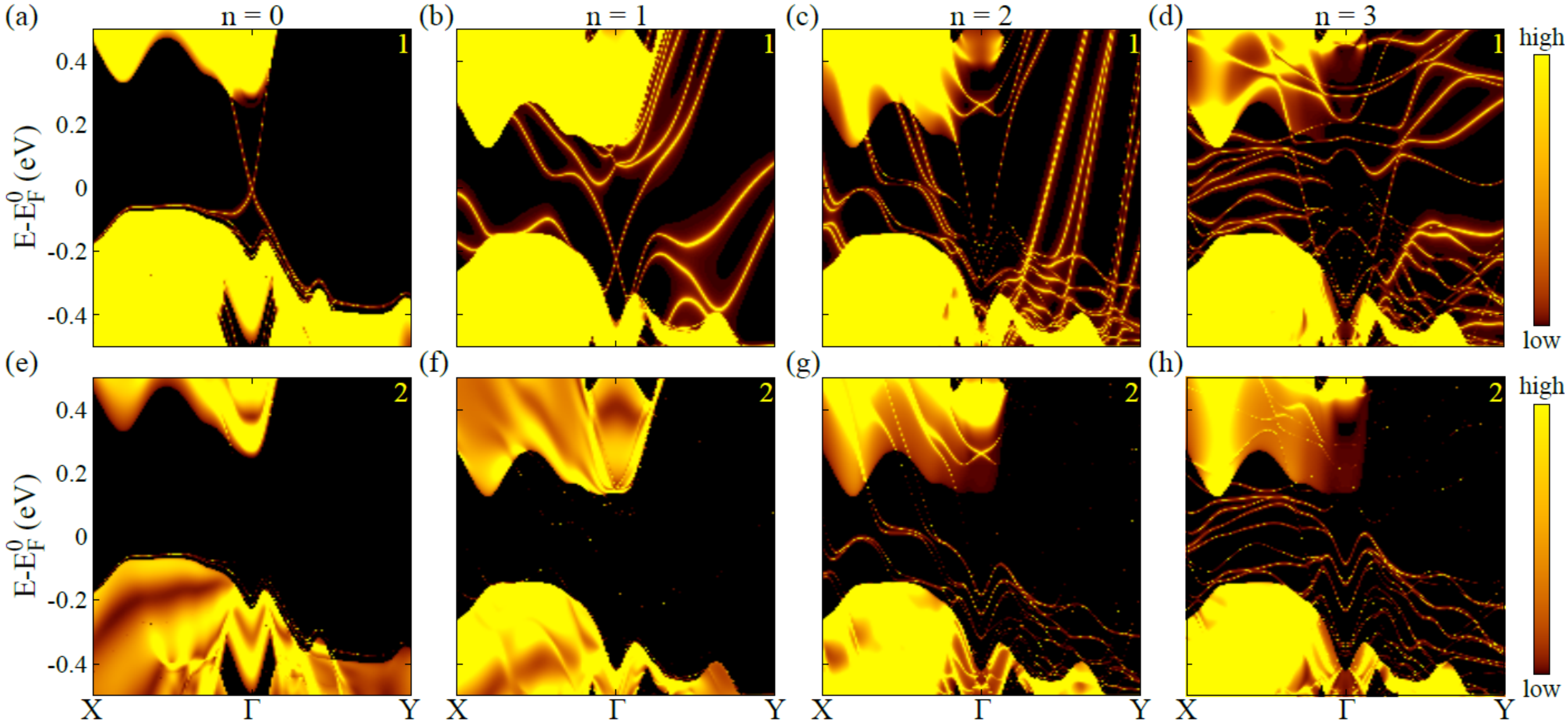

Spin Textures on the TI Side of TI/FM and TI/NM Interfaces

Nano Lett. **17**, 5626 (2017)

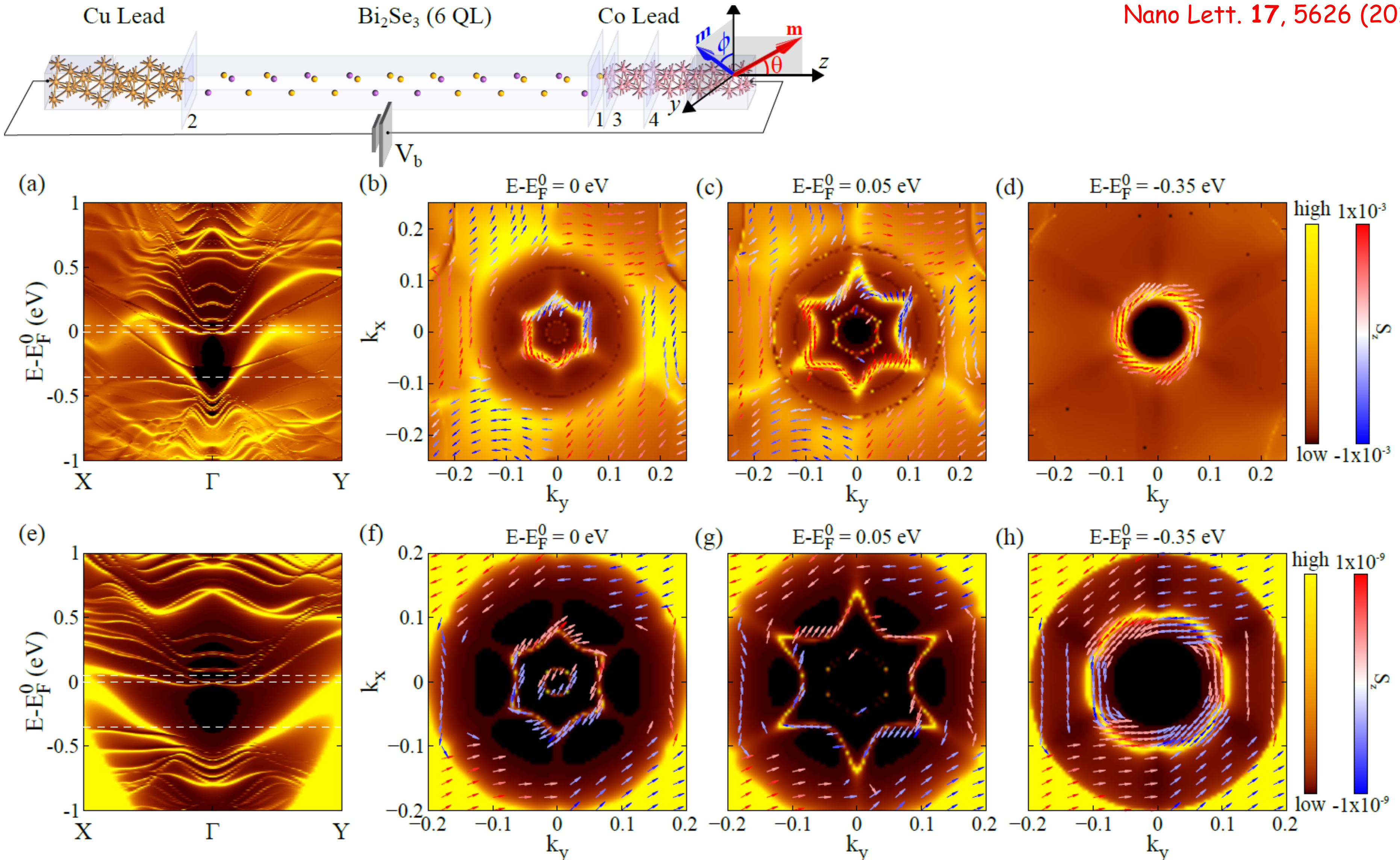

Tunneling Anisotropic Magnetoresistance (TAMR) as a Probe of Interfacial Spin Texture

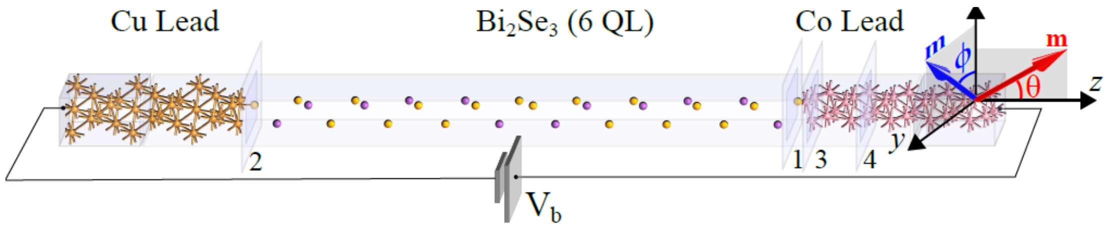

$$\mathrm{TAMR}_{\mathrm{out}}(\theta) = \frac{R(\theta) - R(0)}{R(0)}$$

$$\mathrm{TAMR}_{\mathrm{in}}(\theta) = \frac{R(\phi) - R(0)}{R(0)}$$

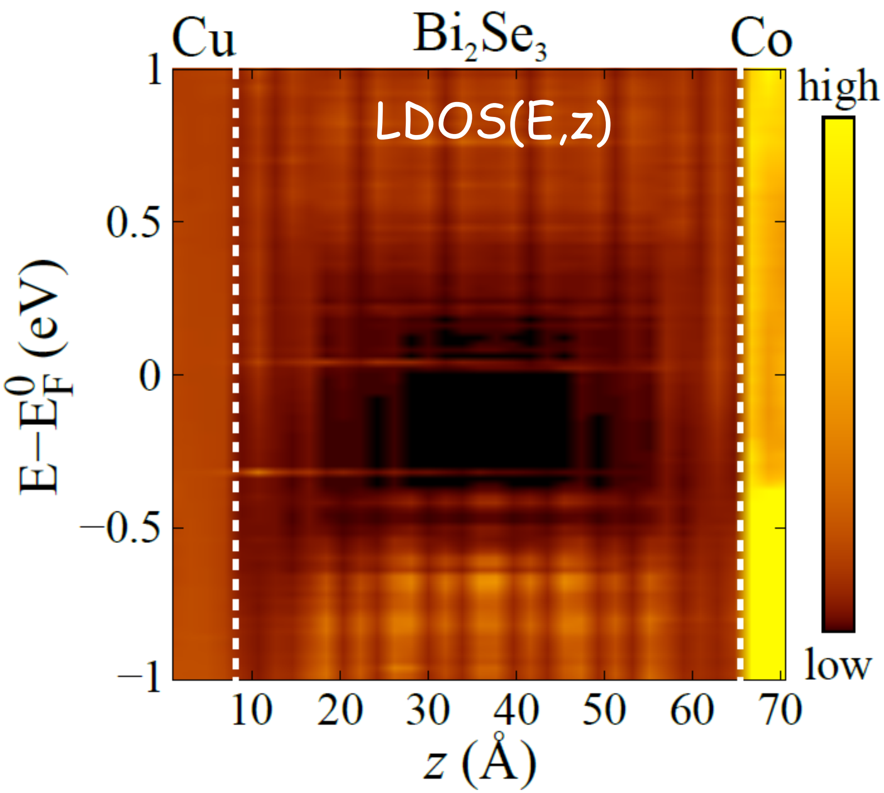

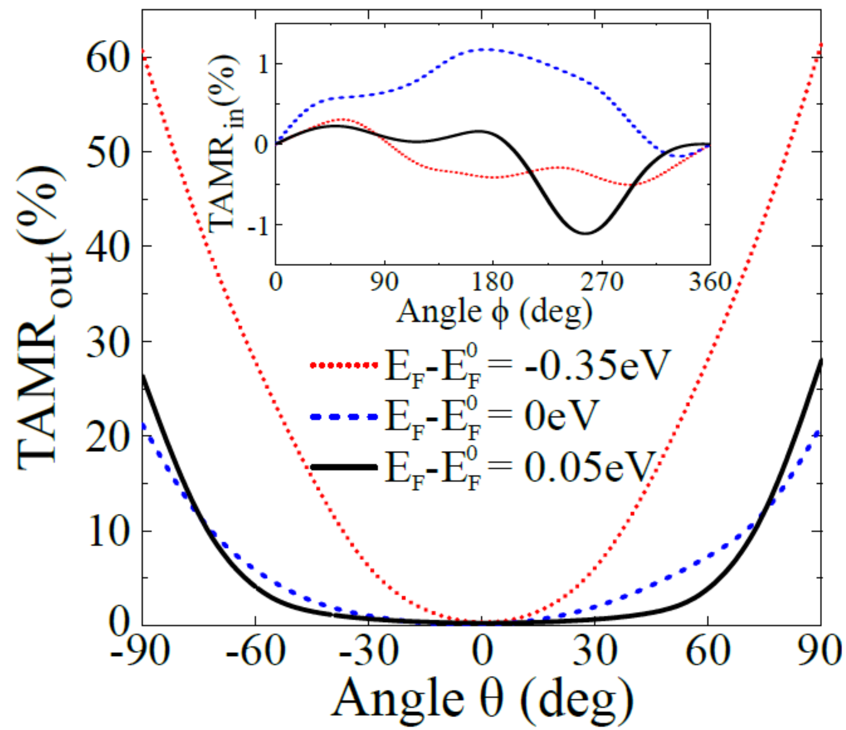

Nano Lett. **17**, 5626 (2017)

Spin-Orbit-Proximitized Ferromagnet: Co/Monolayer-Transition-Metal-Dichalcogenide

Phys. Rev. Mater. **4**, 104007 (2020)

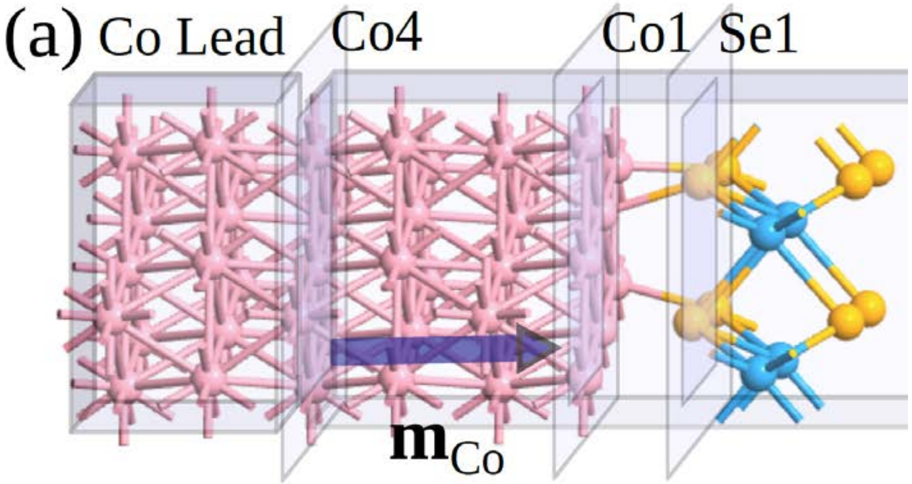

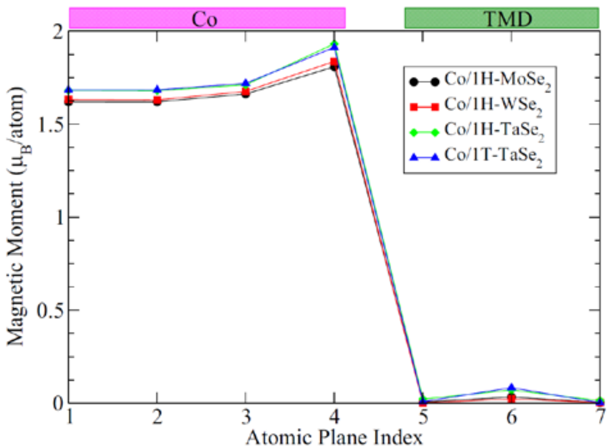

Co/WSe_2

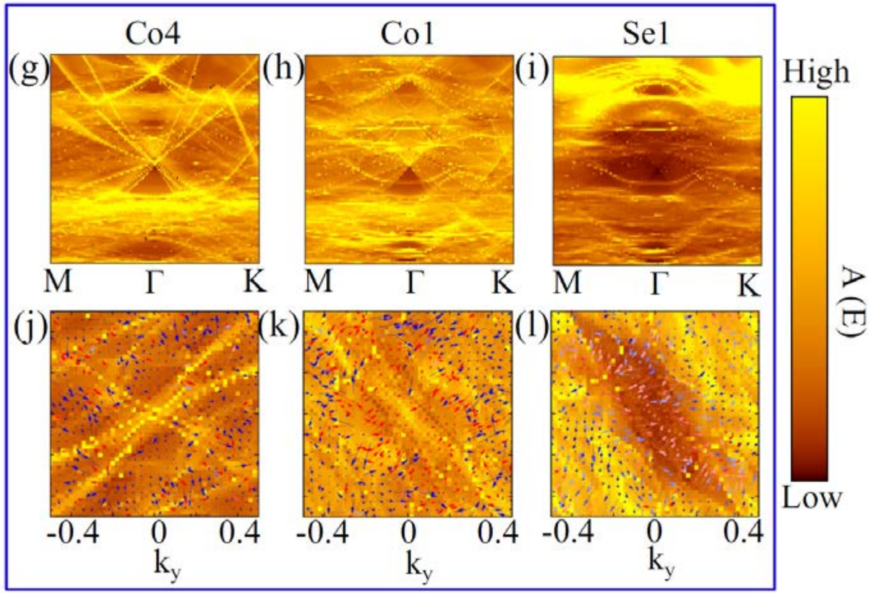

Co/$TaSe_2$

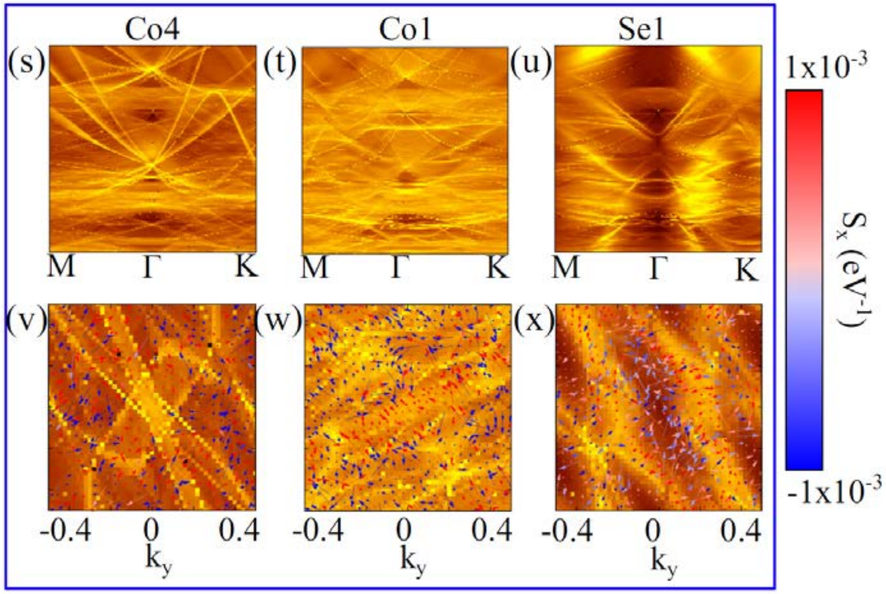

Computational Screening for Optimal SOT in Co/TMD Heterostructures

Nano Lett. **16**, 7514 (2018)

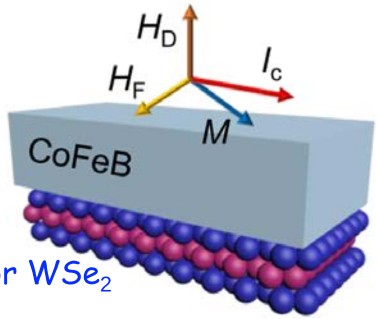

MoS_2 or WSe_2

Nano Lett. **18**, 1311 (2018)

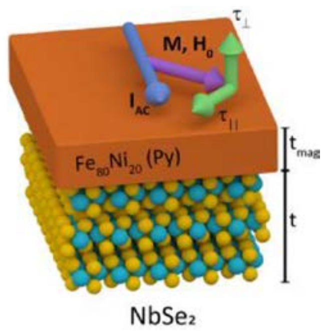

ACS Appl. Mater. Interfaces **10**, 2843 (2018)

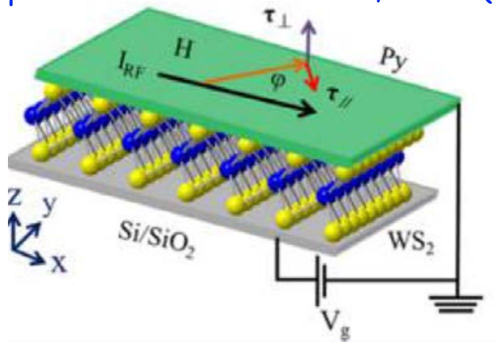

Phys. Rev. Mater. **4**, 104007 (2020)

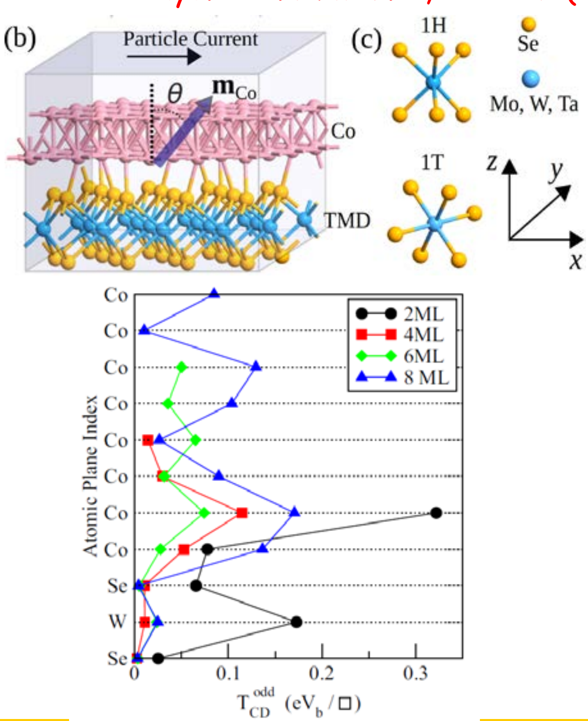

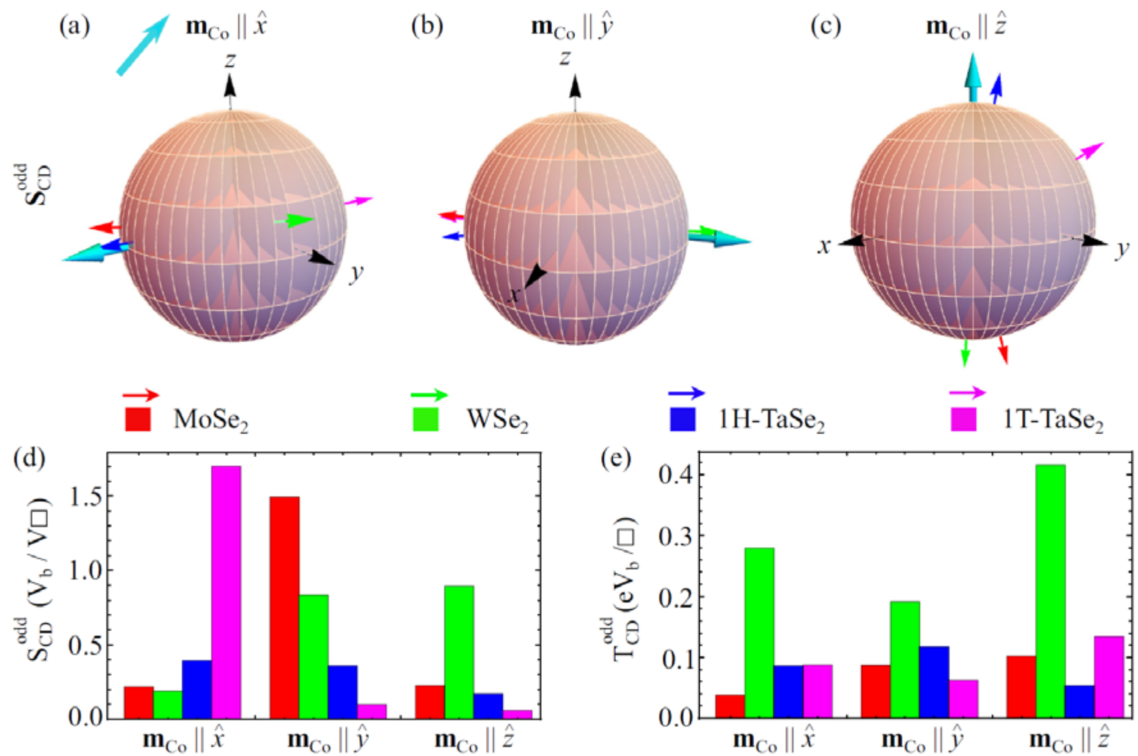

What Can Two-Dimensional (2D) Magnetic Materials do for Spintronics?

Nat. Nanotech. **14**, 408 (2019)

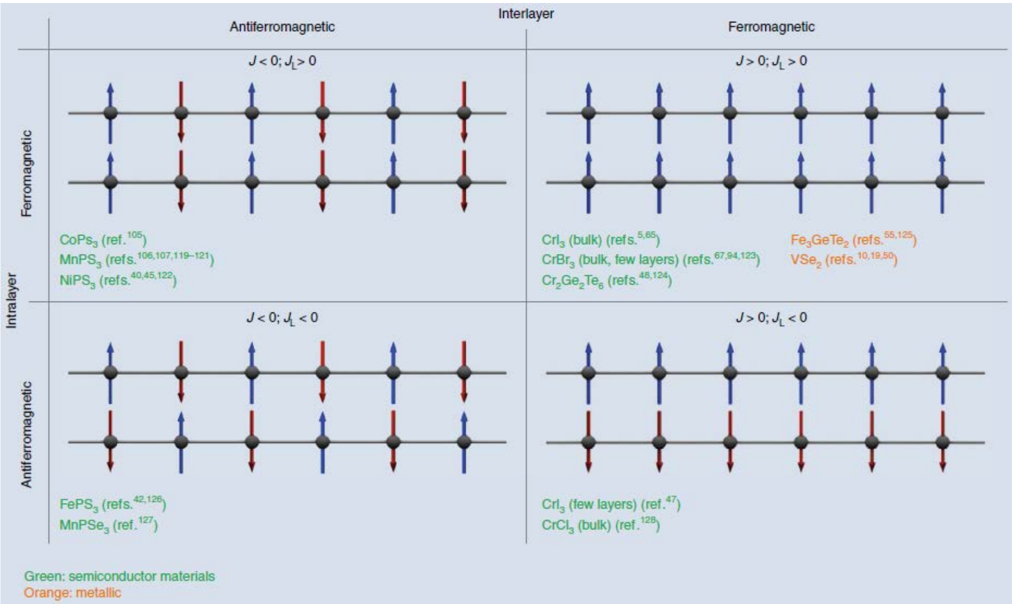

Science **364**, 973 (2019)

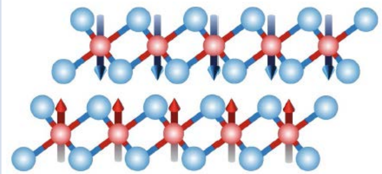

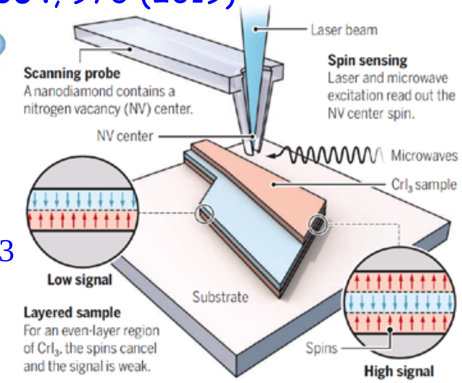

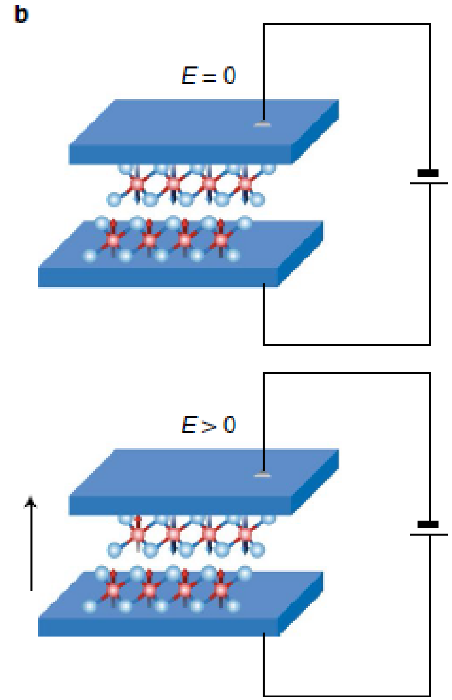

Nat. Mater. **14**, 406 (2018)

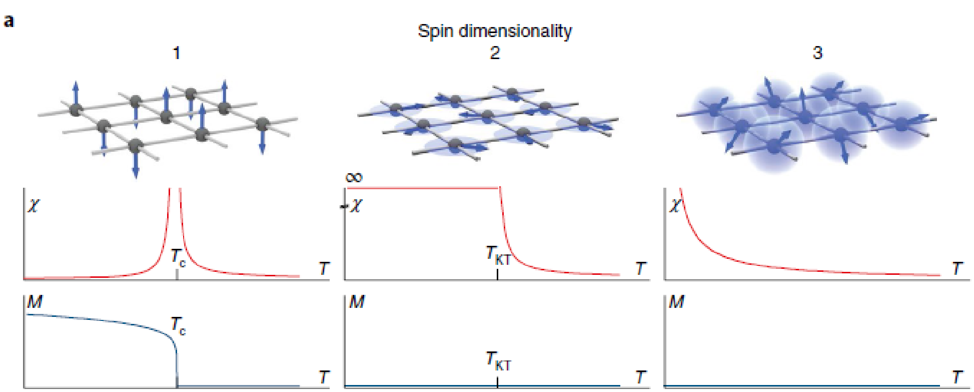

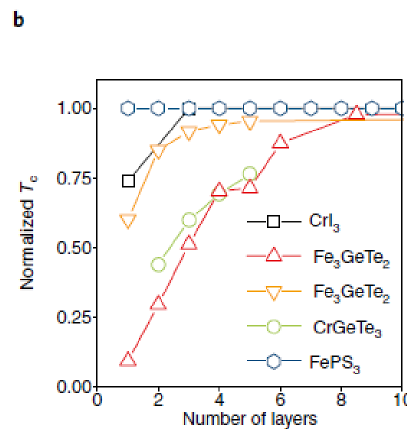

SOT in bilayer-CrI_3/monolayer-$TaSe_2$ vdW Heterostructures

Nano Lett. **20**, 2288 (2020)

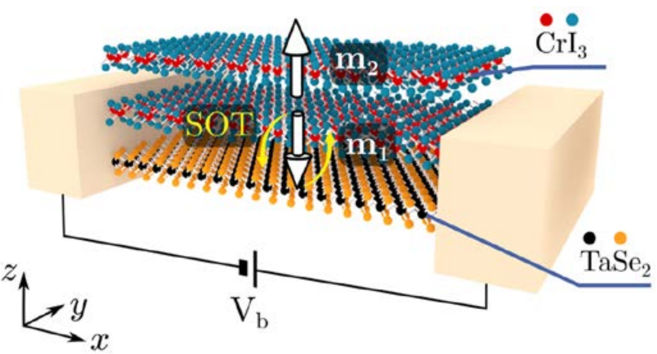

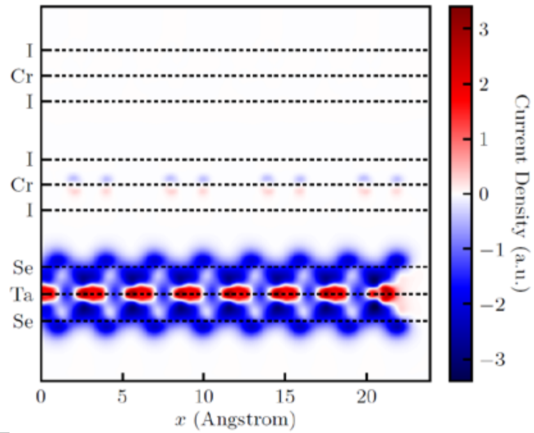

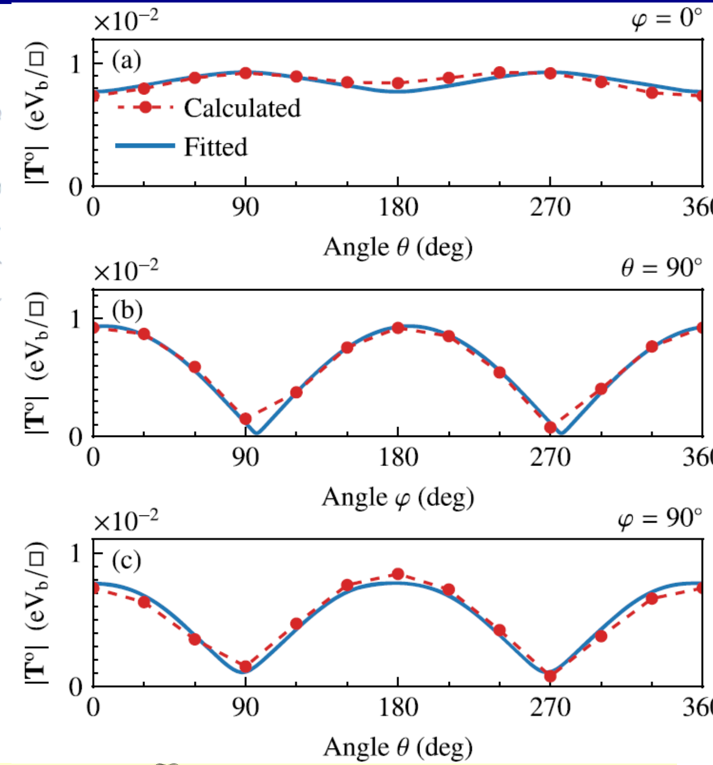

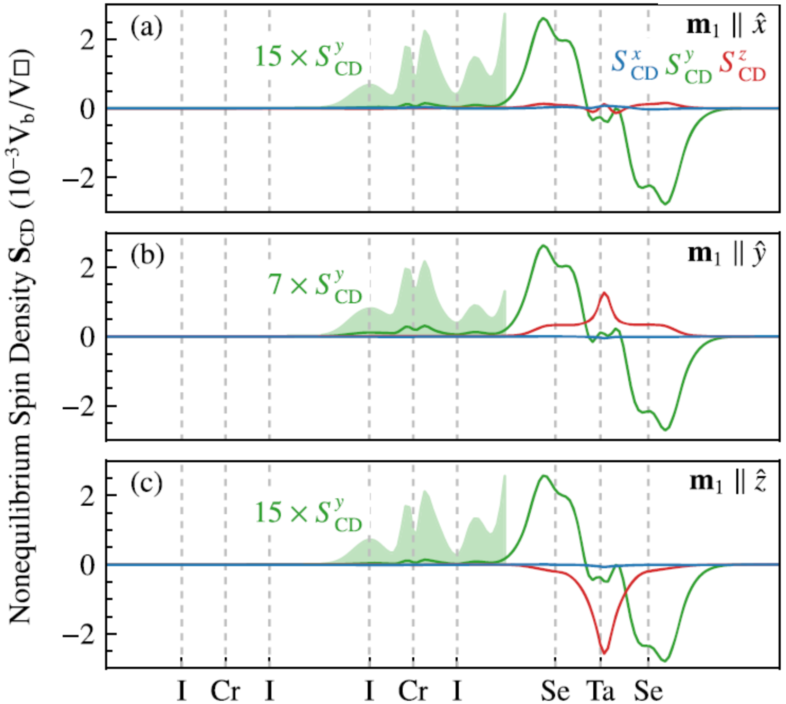

$$
\mathbf{T}^{o} = (\mathbf{p} \times \mathbf{m}_1)\left[\sum_{n=0}^{\infty} \tau^{o}_{n\alpha} |\hat{z} \times \mathbf{m}_1|^{2n}\right] + \mathbf{m}_1 \times (\hat{z} \times \mathbf{m}_1)(\mathbf{m}_1 \cdot \hat{x})\left[\sum_{n=0}^{\infty} \tau^{o}_{n\beta} |\hat{z} \times \mathbf{m}_1|^{2n}\right]
$$

$\mathbf{p}(\theta, \phi)$	$\tau^{o}_{0\alpha}$	$\tau^{o}_{1\alpha}$	$\tau^{o}_{2\alpha}$	$\tau^{o}_{3\alpha}$	$\tau^{o}_{0\beta}$	$\tau^{o}_{1\beta}$
(88°, 98°)	77.22	17.32	-30.32	13.54	-9.19	-6.88

SOT-Driven AFI-FI Nonequilibrium Phase Transition in Bilayer-CrI_3/Monolayer-$TaSe_2$


NANO LETTERS

pubs.acs.org/NanoLett — Letter

Proximity Spin–Orbit Torque on a Two-Dimensional Magnet within van der Waals Heterostructure: Current-Driven Antiferromagnet-to-Ferromagnet Reversible Nonequilibrium Phase Transition in Bilayer CrI_3

Kapildeb Dolui, Marko D. Petrović, Klaus Zollner, Petr Plecháč, Jaroslav Fabian, and Branislav K. Nikolić*

Cite This: *Nano Lett.* 2020, 20, 2288–2295 — Read Online

NEGF+LLG

$$\frac{d\mathbf{m}_1}{dt} = -\gamma \mathbf{m}_1 \times \mathbf{B}_1^{\text{eff}} + \lambda \mathbf{m}_1 \times \frac{d\mathbf{m}_1}{dt} + \frac{\gamma}{\mu_M}\mathbf{T}^{\text{o}}$$

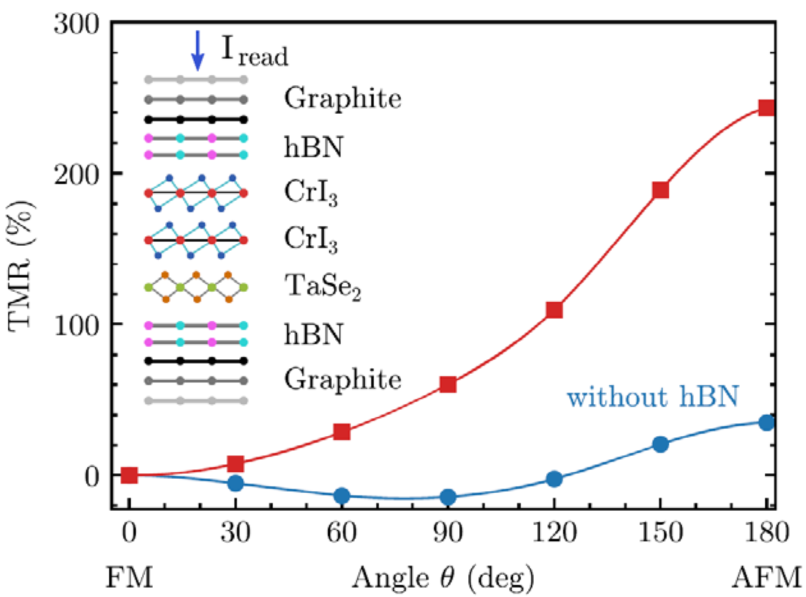

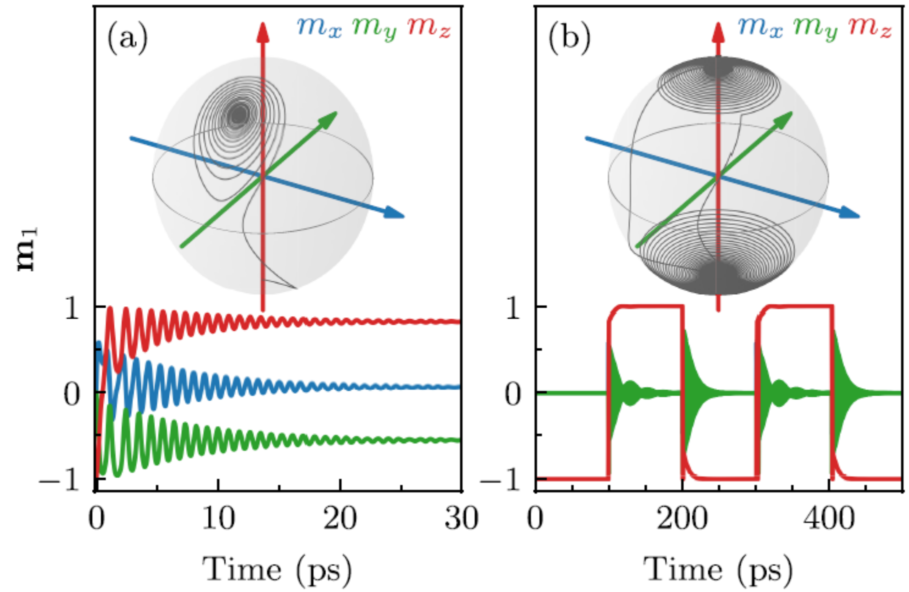

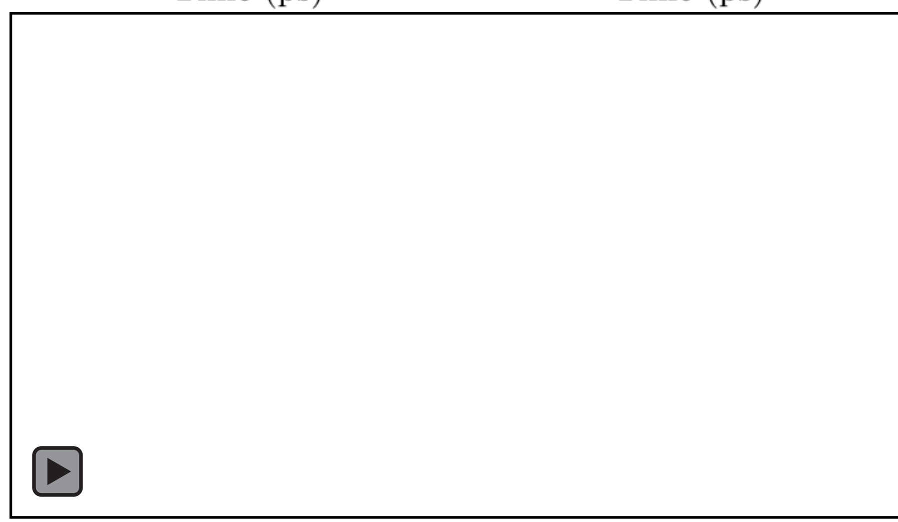

Can We Generate Antidamping SOT Purely from Interfaces <=> in the Absence of SHE?

PHYSICAL REVIEW LETTERS **122**, 077201 (2019)

Spin-Orbit Torques in Heavy-Metal–Ferromagnet Bilayers with Varying Strengths of Interfacial Spin-Orbit Coupling

Lijun Zhu,[1,*] D. C. Ralph,[1,2] and R. A. Buhrman[1]

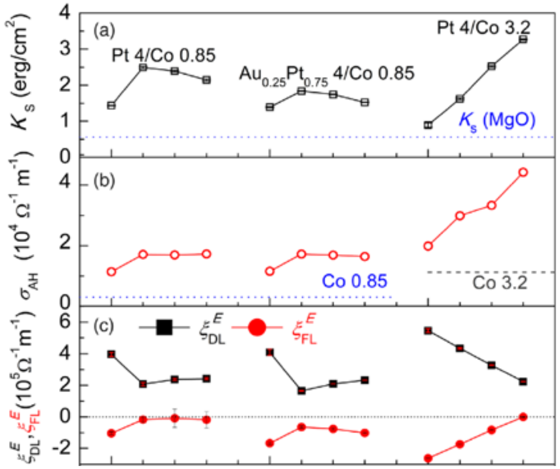

Interfacial contributions to spin-orbit torque and magnetoresistance in ferromagnet/heavy-metal bilayers

K. D. Belashchenko,[1] Alexey A. Kovalev,[1] and M. van Schilfgaarde[2]

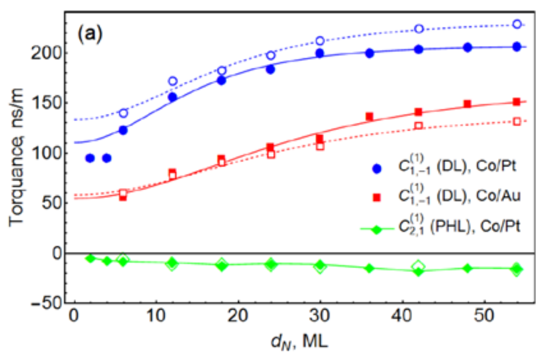

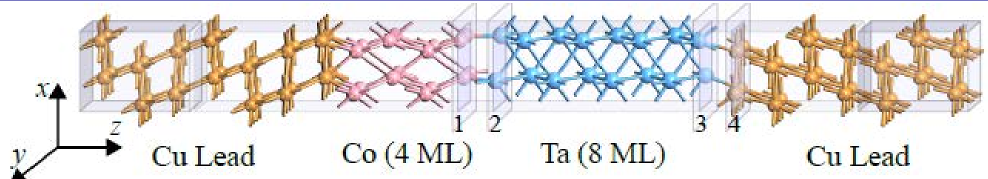

Co/Ta

PRB **96**, 220403(R) (2017)

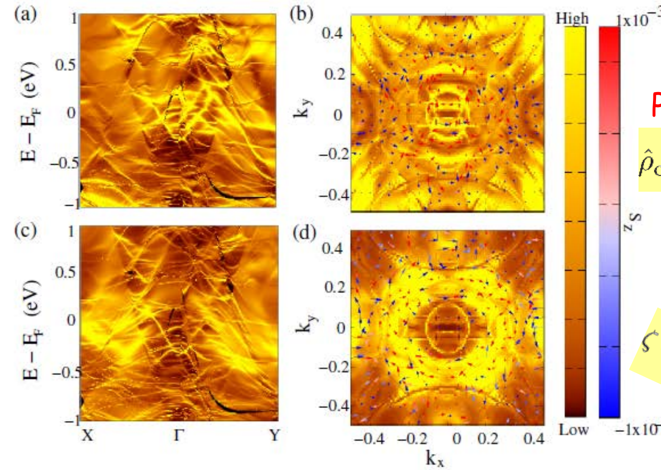

PRB **71**, 195328 (2005)

$$\hat{\rho}_{\mathrm{out(in)}} = \frac{1}{2}\left(1 + \mathbf{P}_{\mathrm{out(in)}} \cdot \hat{\boldsymbol{\sigma}}\right)$$

$$\zeta = \frac{|\mathbf{P}^{\mathrm{out}}_{\mathrm{NM}}|}{|\mathbf{P}^{\mathrm{in}}_{\mathrm{FM}}|} = \frac{|\mathbf{P}^{\mathrm{out}}_{\mathrm{NM}}(d_{\mathrm{HM}} = 1\ \mathrm{ML})|}{|\mathbf{P}^{\mathrm{in}}_{\mathrm{FM}}|}$$

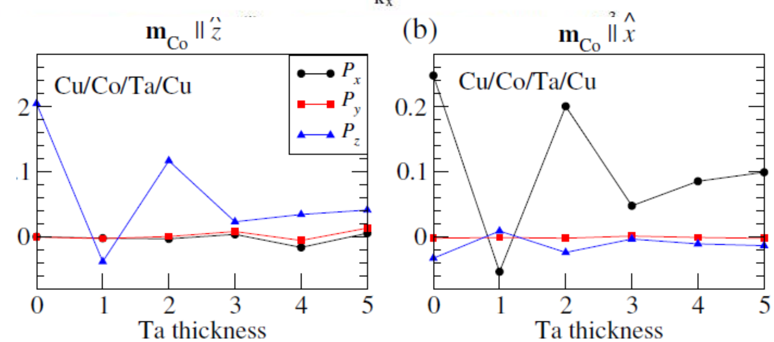

	Cu/Co/Ta/Cu	Co/Ta/Cu	Co/Pt/Cu	Co/Pt/Au	Co/Cu	Co/Au
ζ	0.19 (0.22)	0.57	0.04	0.29	0.70	0.90

Scattering-Induced, Purely Interfacial and Highly Gate-Tunable Damping-Like SOT in Doubly Proximitized Graphene

Phys. Rev. Res. **2**, 043057 (2020)

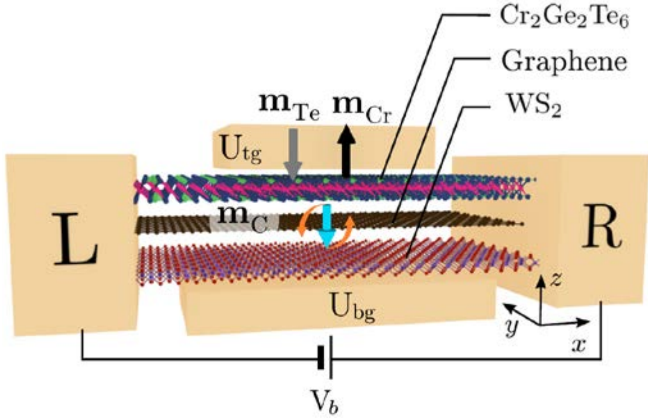

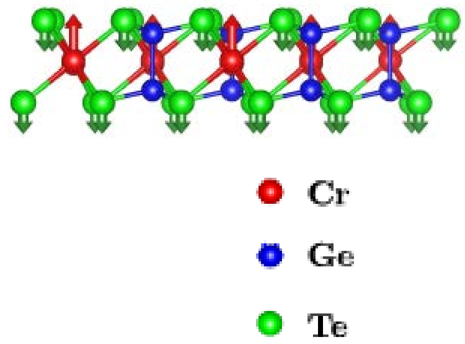

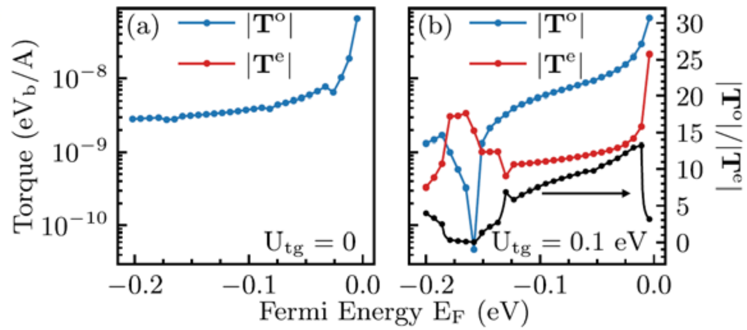

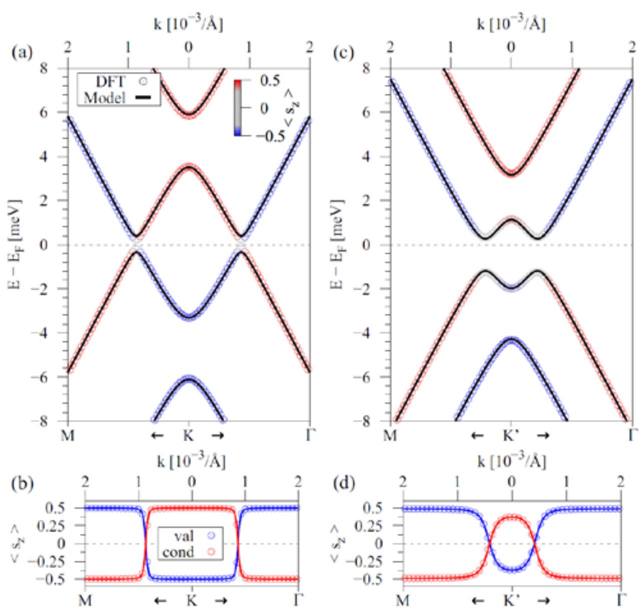

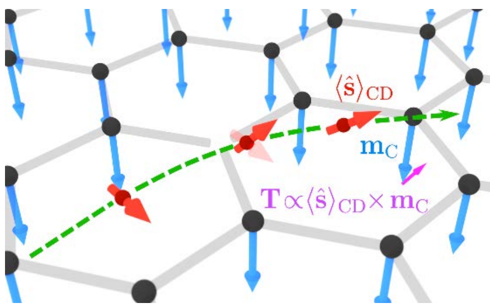

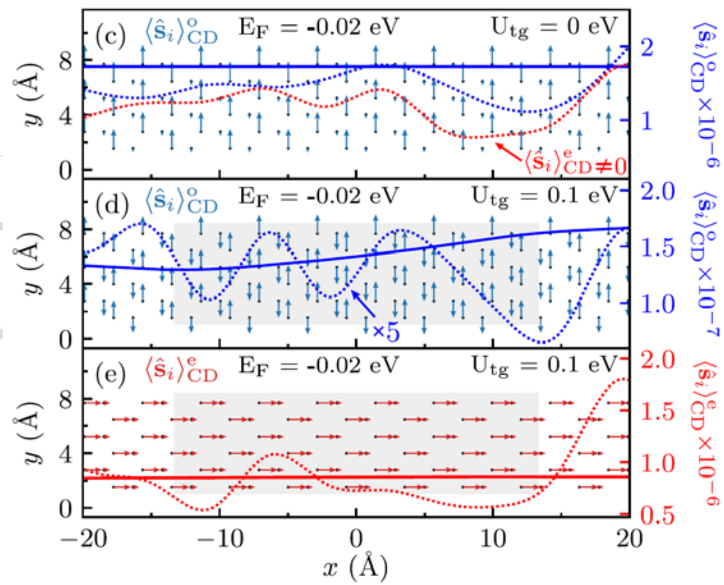

arXiv:2005.09670

Emergent Spin-Orbit Torques in Two-Dimensional Material/Ferromagnet Interfaces

Frederico Sousa,[1] Gen Tatara,[2] and Aires Ferreira[1,*]

Magnon-Mediated STT

Wang *et al.*, *Science* **366**, 1125–1128 (2019)

MAGNONICS

Magnetization switching by magnon-mediated spin torque through an antiferromagnetic insulator

Yi Wang[1,2]*, Dapeng Zhu[1]*, Yumeng Yang[1], Kyusup Lee[1], Rahul Mishra[1], Gyungchoon Go[3], Se-Hyeok Oh[4], Dong-Hyun Kim[5], Kaiming Cai[1], Enlong Liu[1], Shawn D. Pollard[1], Shuyuan Shi[1], Jongmin Lee[1], Kie Leong Teo[1], Yihong Wu[1], Kyung-Jin Lee[3,4,5,6], Hyunsoo Yang[1]†

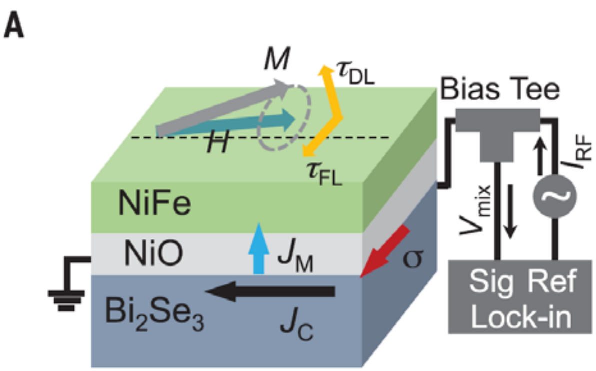

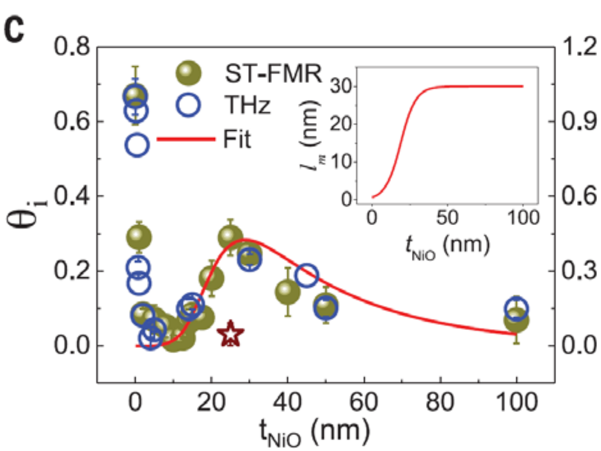

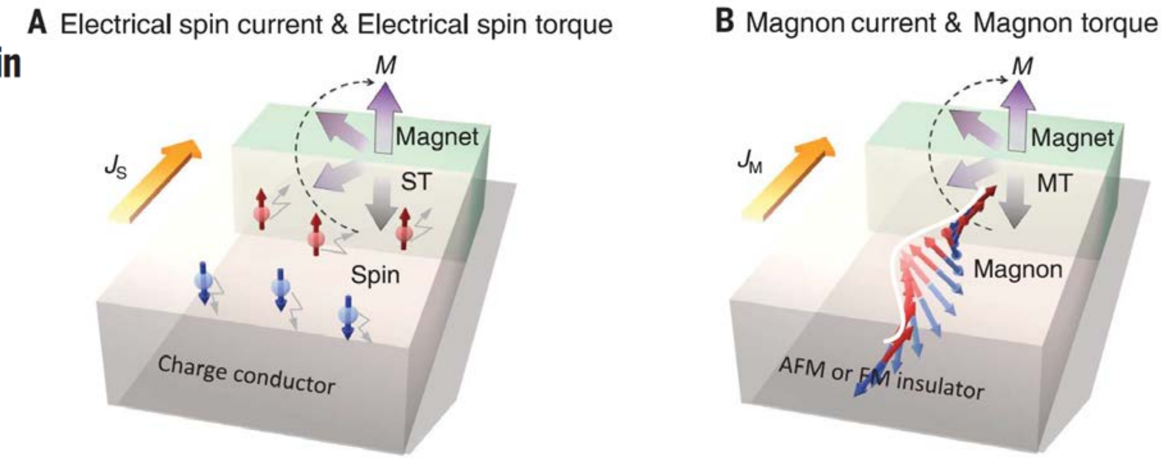

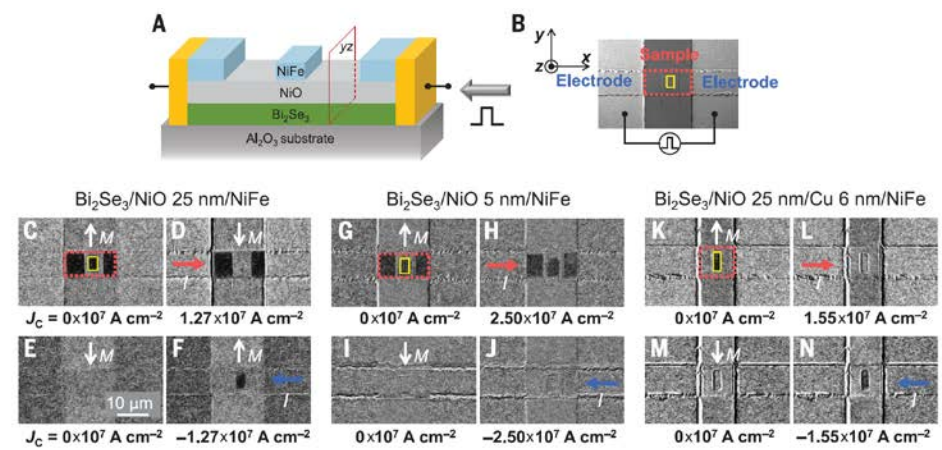

Fig. 4. Magnetization switching induced by magnon torque in the Bi_2Se_3/NiO/Py devices at room temperature. (**A**) Illustration of the structure of the magnon torque switching device with an isolated Py rectangle defined on top of the NiO layer. (**B**) Optical microscope image of a device with electrodes, where the sample functional region is indicated with a red dotted box and an isolated Py rectangle is denoted with a yellow box. (**C** to **F**) MOKE images for magnon-torque-driven magnetization switching in the Bi_2Se_3/NiO (25 nm)/Py device by injecting a pulsed current I along the [(C) and (D)] +x axis or [(E) and (F)] −x axis at room temperature. (**G** to **J**) MOKE images for a Bi_2Se_3/NiO (5 nm)/Py device by injecting I along the [(G) and (H)] +x axis or [(I) and (J)] −x axis at room temperature. (**K** to **N**) MOKE images for the Bi_2Se_3/NiO (25 nm)/Cu (6 nm)/Py device by injecting I along the [(K) and (L)] +x axis or [(M) and (N)] −x axis at room temperature. In (C) to (N), the dark contrast represents the magnetization along the +y axis, and the light contrast represents the magnetization along the −y axis. The direction of magnetization is indicated with white arrows. The current density J_c in the Bi_2Se_3 layer is denoted underneath each image.

Magnons and Magnonics

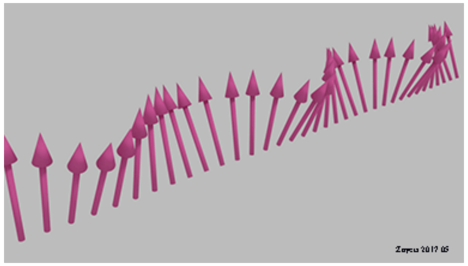

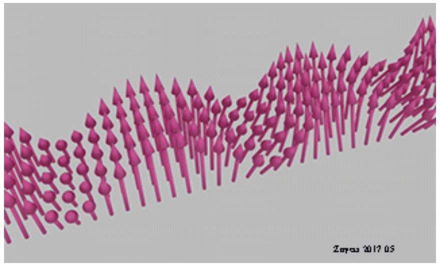

nature physics

REVIEW ARTICLE

PUBLISHED ONLINE: 2 JUNE 2015 | DOI: 10.1038/NPHYS3347

Magnon spintronics

A. V. Chumak*, V. I. Vasyuchka, A. A. Serga and B. Hillebrands

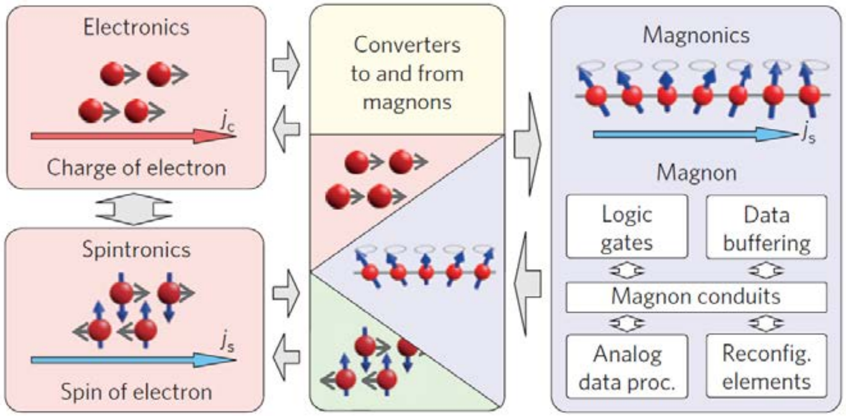

Box 1 | Data processing benefiting from magnonics.

Wave-based computing. A promising direction for a future beyond-CMOS computing technology (CMOS: complementary metal–oxide–semiconductor) is based on the substitution of electrons by quasi-particles such as magnons or photons[7–9], which allow operations with vector rather than scalar variables. The usage of wave phase provides an additional degree of freedom in data processing[10–13], opens the way to non-Boolean computing algorithms[14,15], and allows a decrease in footprint of the computing elements[16]. A good example is a majority gate produced in the form of a three-input combiner[12,16,17], which substitutes several tens of CMOS transistors. Reversible logic[18,19] and parallel computing, where the same element simultaneously processes data at different frequencies[20], are other advantages.

Insulator-based spintronics. A magnon current has advantages as compared to a conventional spin-polarized electron current. It does not involve the motion of electrons and, thus, it is free of Joule heat dissipation[7]. In low-damping magnetic dielectrics (for example, yttrium-iron-garnet, YIG; ref. 21) magnons can propagate over centimetre distances[22] whereas an electron-carried spin current is limited by the spin diffusing length, which does not exceed one micrometre.

Wide frequency range from GHz to THz. The wave frequency defines the maximum clock rate of a computing device. The magnon spectrum covers the GHz frequency range used nowadays in communication[5,6], and it reaches into the very promising THz range[21,23,24]. For example, the edge of the first magnonic Brillouin zone in YIG lies at about 7 THz (ref. 21).

Nanosized structural elements. The minimal sizes of wave-based computing elements are defined by the wavelength of the used wave. Spin waves are promising because they allow operations with wavelengths below 10 nm (a lower limit is given by the lattice constant of a specific magnetic material[21,23,24]). Moreover, the frequency of exchange magnons increases quadratically with decreasing wavelength, and their group velocity increases linearly in the first one-third of the Brillouin zone. Thus, miniaturization[25,26] of magnon-based devices goes along with an increase in computing speed (see discussions in ref. 7).

Contactless wiring. Wiring, which is required for powering of separate elements, increases the complexity of the architecture and occupies a significant part of the chip area. Feeding of magnonic elements can be realized using an electro-magnetic wave: Au *et al.* proposed placing a magnonic chip in a global microwave field driving a number of separate, local spin-wave transducers[27].

Wide physical toolbox. Magnon properties can be engineered on a broad scale by a choice of the magnetic material, the strength of a magnetic field, the magnetization direction, the geometry of magnetic structures, and so on. In addition, there is a variety of physical effects applicable for the control of spin-wave excitation and propagation. For example, nonreciprocal operations required in communications[28] and logic devices[29] can be realized by the use of the magnetostatic surface waves (MSSWs; refs 2,3): an antenna excites a MSSW packet in one propagation direction only[29–31]. Another example is a spin-wave wavelength converter[32], which uses the change in the geometry of a spin-wave conduit to reduce the magnon wavelength. Spatial addressing of magnon currents is possible even in a plane film: spin-wave caustics[33,34] can be used for the formation of non-diffractive wave beams. The direction of these beams is controlled by the magnetic field.

Nonlinear data processing. A wide variety of pronounced nonlinear spin-wave effects[2–4,22], opens additional opportunities for data processing. For example, data can be transferred over large distances without distortion in the form of spin-wave solitons[35] and bullets[36], or they can be buffered in non-propagating modes and restored afterwards[37]. Effects such as wavefront reversal[36,38] and power limiting[39] have been demonstrated. Finally, the nonlinearity of magnons allows the control of one magnon current by another and, thus, the realization of magnon transistors[7].

Macroscopic quantum phenomena. Magnons are bosons and can form a Bose–Einstein condensate—a spontaneous coherent ground state—established independently of the magnon excitation mechanism even at room temperature[40,41]. A magnon supercurrent, a collective motion of condensed magnons driven by a phase gradient of a condensate wavefunction[42], can be used for low-loss information transfer. Recent theoretical predictions address the magnonic Josephson effect[43] and the magnon Aharonov–Casher effect, where the supercurrent is controlled by an electric field[44].

TDNEGF+LLG Approach Tested on Familiar Example of Electron-Mediated STT

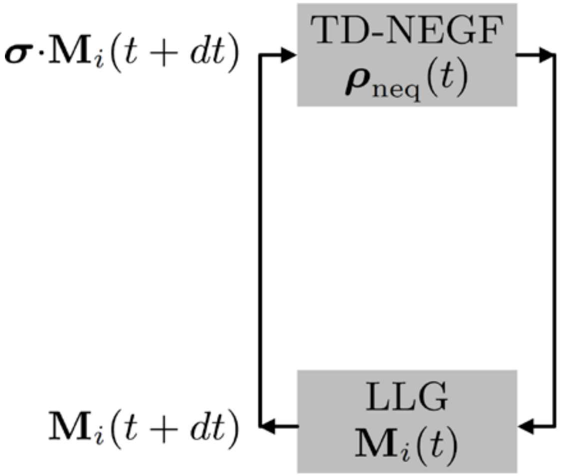

$$\mathbf{S}^i_{\rm CD}(t) = \mathbf{S}^i_{\rm neq}(t) - \mathbf{S}^i_{\rm eq}$$

quantum Hamiltonian for electrons

$$\hat{H}_{\rm TB} = -\gamma \sum_{\langle ij \rangle} \hat{c}_i^\dagger \hat{c}_j - J_{sd} \sum_i \hat{c}_i^\dagger \boldsymbol{\sigma} \cdot \mathbf{M}_i(t) \hat{c}_i$$

classical Hamiltonian for local magnetic moments

$$\mathcal{H}_{\rm CL} = -J \sum_{\langle ij \rangle} \mathbf{M}_i \cdot \mathbf{M}_j - J_{sd} \sum_i \mathbf{S}^i_{\rm CD} \cdot \mathbf{M}_i - K \sum_i (M_i^z)^2 + D \sum_i (M_i^y)^2$$

$$\mathbf{S}^i_{\rm CD}(t) \times \mathbf{M}_i(t)$$


PHYSICAL REVIEW APPLIED **10,** 054038 (2018)

Editors' Suggestion

Spin and Charge Pumping by a Steady or Pulse-Current-Driven Magnetic Domain Wall: A Self-Consistent Multiscale Time-Dependent Quantum-Classical Hybrid Approach

Marko D. Petrović,[1] Bogdan S. Popescu,[2] Utkarsh Bajpai,[2] Petr Plecháč,[1] and BranislavK. Nikolić[2,*,†]

[1] *Department of Mathematical Sciences, University of Delaware, Newark, Delaware 19716, USA*
[2] *Department of Physics and Astronomy, University of Delaware, Newark, Delaware 19716, USA*

- Time-dependent nonequilibrium density matrix:

$$\boldsymbol{\rho}_{\rm neq}(t) = \frac{\hbar}{i} \mathbf{G}^<(t,t')\Big|_{t=t'}$$

$$i\hbar \frac{d\boldsymbol{\rho}_{\rm neq}}{dt} = [\mathbf{H}_{\rm TB}, \boldsymbol{\rho}_{\rm neq}] + i \sum_{p={\rm L,R}} [\boldsymbol{\Pi}_p(t) + \boldsymbol{\Pi}_p^\dagger(t)]$$

$$\boldsymbol{\Pi}_p(t) = \int_{t_0}^{t} dt_2 \, [\mathbf{G}^>(t,t_2)\boldsymbol{\Sigma}_p^<(t_2,t) - \mathbf{G}^<(t,t_2)\boldsymbol{\Sigma}_p^>(t_2,t)]$$

- Nonequilibrium spin density and spin torque:

$$\mathbf{S}^i_{\rm CD}(t) = \frac{\hbar}{2}{\rm Tr}_{\rm spin}[\boldsymbol{\rho}_{\rm neq}(t)\boldsymbol{\sigma}] - \frac{\hbar}{2}{\rm Tr}_{\rm spin}[\boldsymbol{\rho}_{\rm eq}\boldsymbol{\sigma}]$$

$$\mathbf{T}_i(t) \propto \mathbf{S}^i_{\rm CD}(t) \times \mathbf{M}_i(t)$$

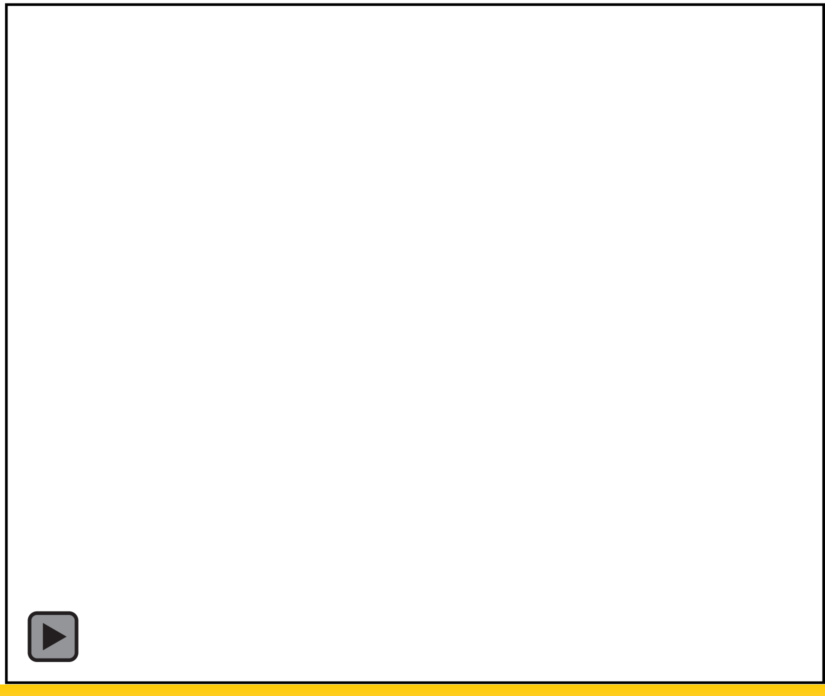

How Important is Noncommutativity of Hamiltonian at Different Times That is Absent in Naïve NEGF+LLG?

arXiv:2008.02794

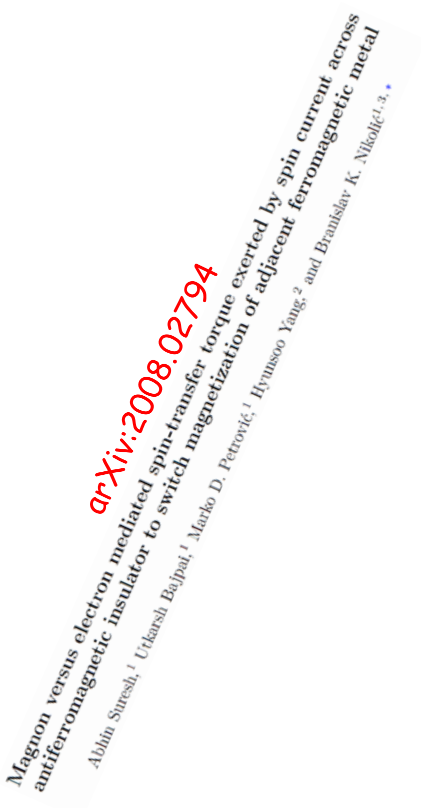
Magnon versus electron mediated spin-transfer torque exerted by spin current across antiferromagnetic insulator to switch magnetization of adjacent ferromagnetic metal

Abhin Suresh,[1] Utkarsh Bajpai,[1] Marko D. Petrović,[1] Hyunsoo Yang,[2] and Branislav K. Nikolić[1,3,*]

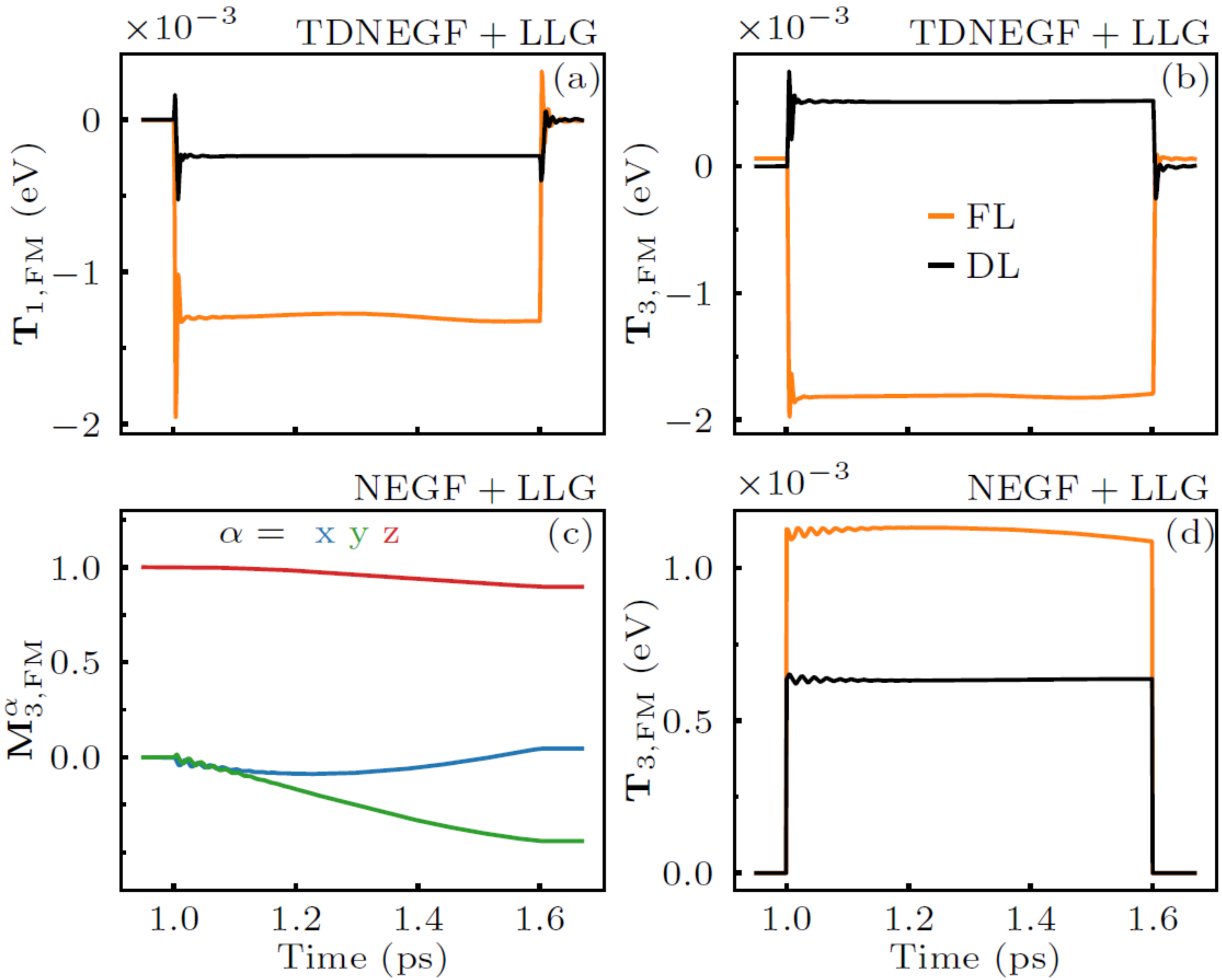

TDNEGF+LLG Approach to Magnon-Mediated STT in FM/AFI/FM Junctions

arXiv:2008.02794

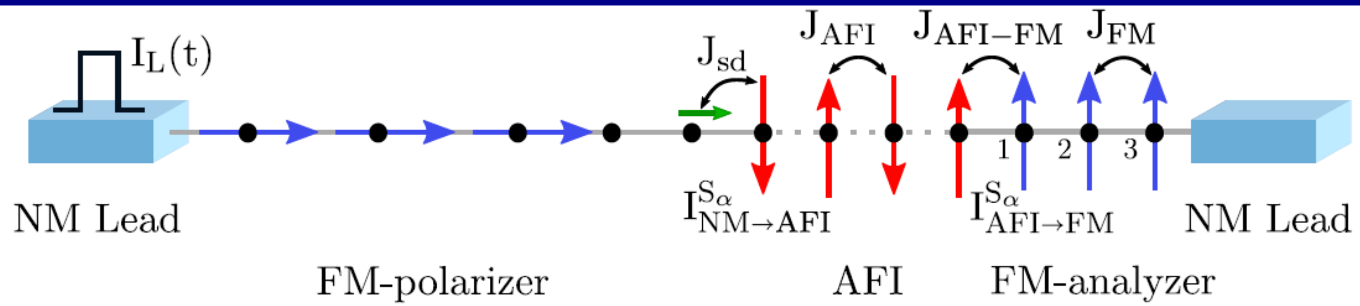

Why is the AFI Injecting Spin Current Into FM: Spin Pumping by Magnetization Dynamics

Charge Pumping

An Adiabatic Quantum Electron Pump

M. Switkes,[1] C. M. Marcus,[1*] K. Campman,[2] A. C. Gossard[2]

Science **283**, 1905 (1999)

requires quantum-coherence and low temperatures + very difficult to disentangle from other competing effects

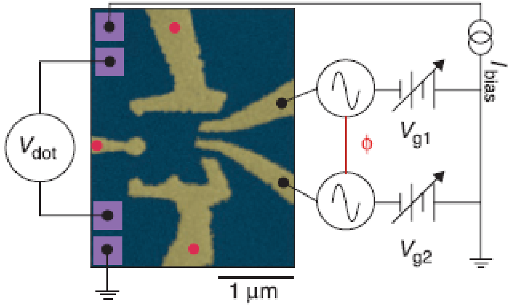

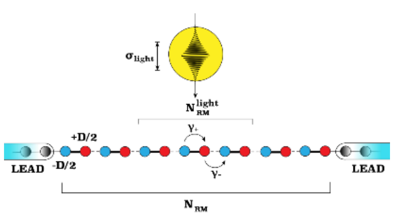

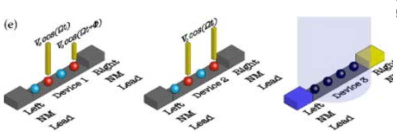

J. Phys.: Mater. 2 (2019) 025004

JPhys Materials

PAPER

Spatio-temporal dynamics of shift current quantum pumping by femtosecond light pulse

U Bajpai, B S Popescu, P Plecháč, B K Nikolić, L E F Foa Torres, H Ishizuka and N Nagaosa

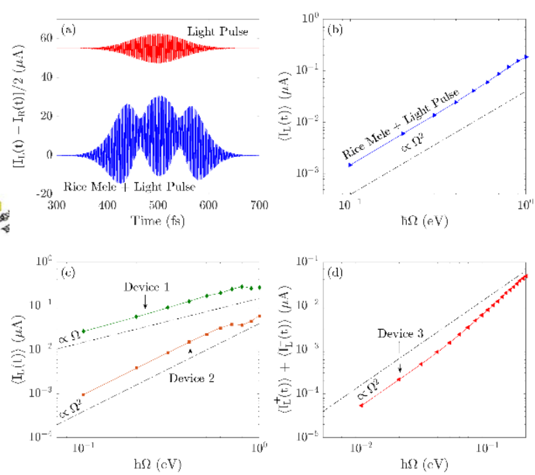

Spin Pumping

IOP Publishing

Semiconductor Science and Technology

Semicond. Sci. Technol. 29 (2014) 043002 (13pp)

doi:10.1088/0268-1242/29/4/043002

Invited Review

Dynamical generation of spin currents

Kazuya Ando

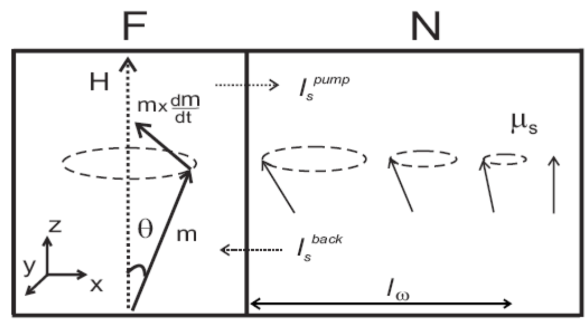

robust and ubiquitous effect in magnetic heterostructures even at room temperature

Experimental manifestations

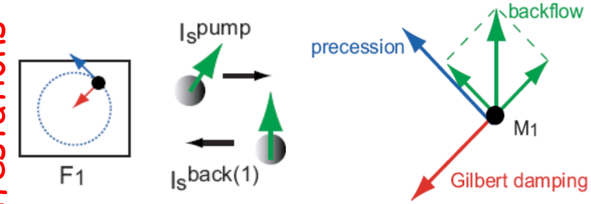

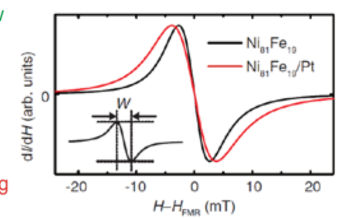

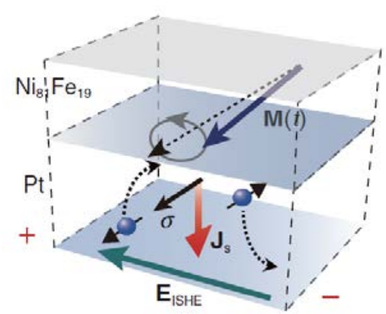

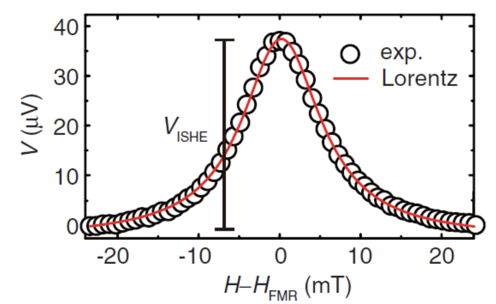

1D Tight-Binding Model of Spin Pumping: Landauer-Büttiker Formula in Rotating Frame

PHYSICAL REVIEW B **79**, 054424 (2009)

Spin and charge pumping in magnetic tunnel junctions with precessing magnetization: A nonequilibrium Green function approach

Son-Hsien Chen,[1,2,*] Ching-Ray Chang,[2,†] John Q. Xiao,[1] and Branislav K. Nikolić[1]

PHYSICAL REVIEW B **82**, 195440 (2010)

Microwave-driven ferromagnet–topological-insulator heterostructures: The prospect for giant spin battery effect and quantized charge pump devices

Farzad Mahfouzi,[1] Branislav K. Nikolić,[1,2] Son-Hsien Chen,[1,2,*] and Ching-Ray Chang[2,†]

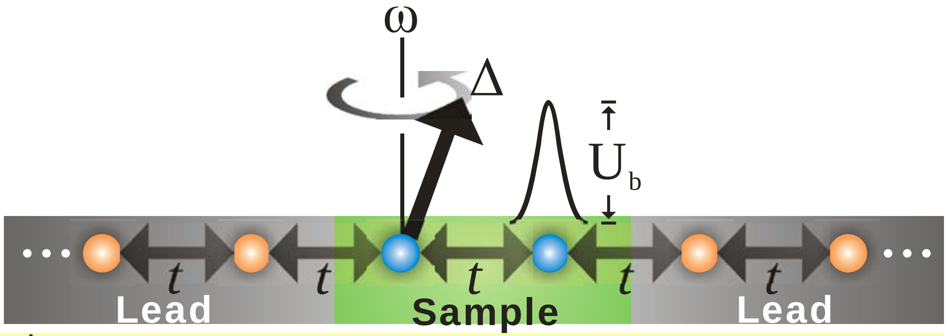

$$\hat{H}_{\rm lab}(t) = \sum_{\mathbf{r},\sigma,\sigma'} \left(\varepsilon_{\mathbf{r}} \delta_{\sigma\sigma'} - \frac{\Delta_{\mathbf{r}}}{2} \mathbf{m}_{\mathbf{r}}(t) \cdot \hat{\boldsymbol{\sigma}}^{\sigma\sigma'} \right) \hat{c}^\dagger_{\mathbf{r}\sigma} \hat{c}_{\mathbf{r}\sigma'} - \gamma \sum_{\langle \mathbf{r}\mathbf{r}' \rangle \sigma} \hat{c}^\dagger_{\mathbf{r}\sigma} \hat{c}_{\mathbf{r}'\sigma}$$

$$\hat{H}_{\rm rot} = \hat{U} \hat{H}_{\rm lab}(t) \hat{U}^\dagger - i\hbar \hat{U} \frac{\partial}{\partial t} \hat{U}^\dagger = \hat{H}_{\rm lab}(0) - \frac{\hbar\omega}{2} \hat{\sigma}_z$$

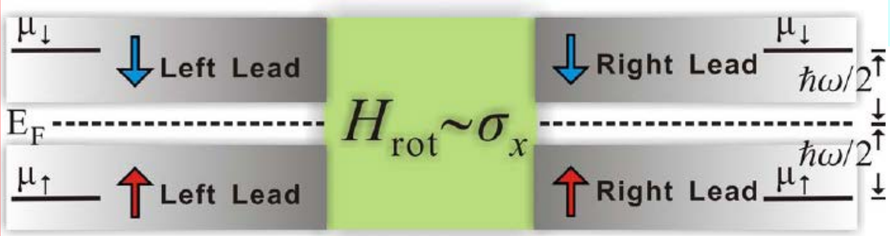

$$I_L^S = \frac{e\omega}{2\pi} \int_{\rm BZ} d\mathbf{k}_{||} \, (T_{LR}^{\uparrow\downarrow} + T_{RL}^{\uparrow\downarrow} + 2T_{LL}^{\uparrow\downarrow})$$

$$I = \frac{e\omega}{2\pi} \int_{\rm BZ} d\mathbf{k}_{||} \, (T_{RL}^{\uparrow\downarrow} - T_{LR}^{\uparrow\downarrow})$$

$$V_{\rm pump} = I G(\theta)^{-1}$$

Exact Solution for Adiabatic Spin and Nonadiabatic Charge Pumped Currents

PRB **79**, 054424 (2009)

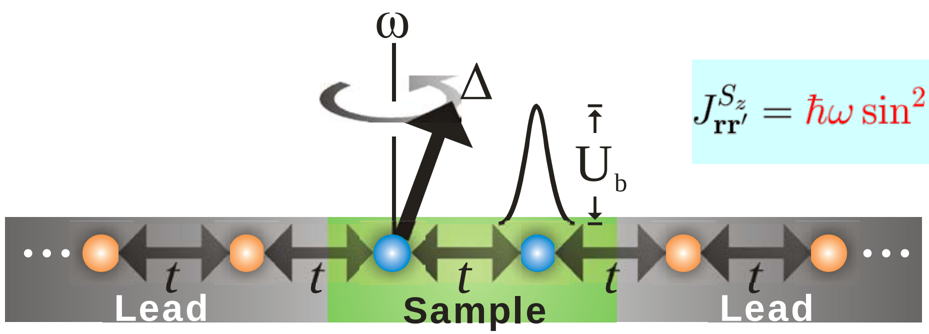

$$J^{S_z}_{\mathbf{rr'}} = \hbar\omega \sin^2\theta\,\Delta^2 \frac{\gamma^2(\mathrm{Im}\,\Sigma_{1\mathrm{D}})^2}{8\pi|R|^2}\left[4\left(\gamma^2+\varepsilon_I^2\right)+4|\Sigma_{1\mathrm{D}}|^2-8\varepsilon_I\mathrm{Re}\,\Sigma_{1\mathrm{D}}\right]$$

Spin current pumping from a single precesing spin

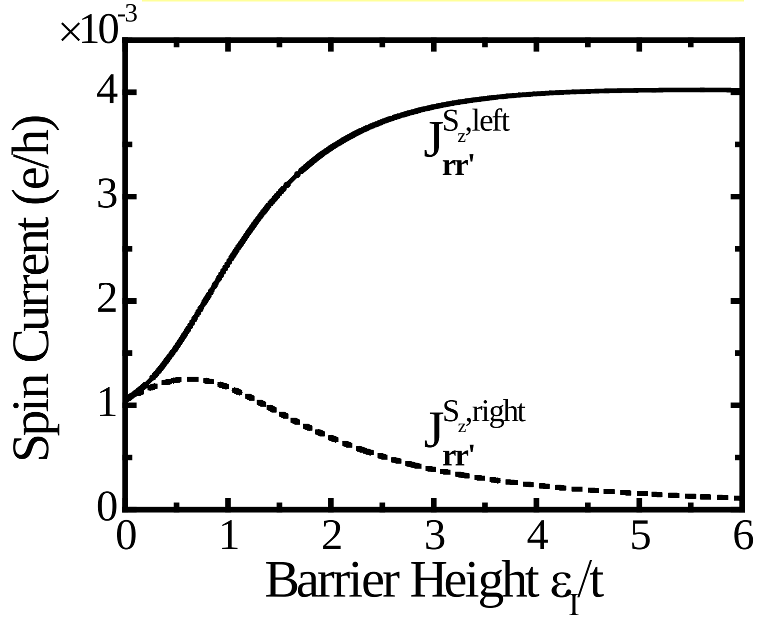

Charge current pumping from a single precesing spin